

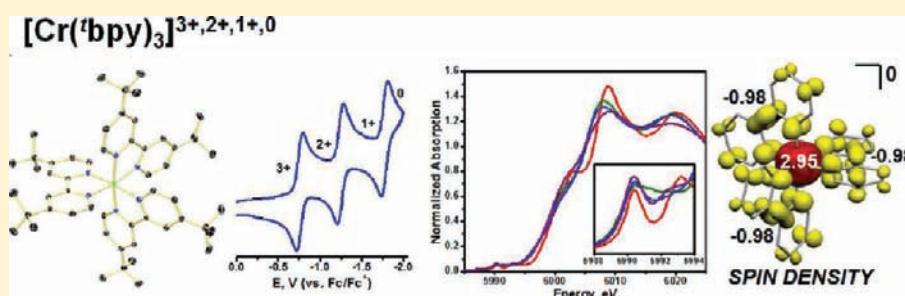
Electronic and Molecular Structures of the Members of the Electron Transfer Series $[\text{Cr}(\text{bpy})_3]^n$ ($n = 3+, 2+, 1+, 0$): An X-ray Absorption Spectroscopic and Density Functional Theoretical Study

Christopher C. Scarborough,^{†,‡} Stephen Sproules,^{†,§} Thomas Weyhermüller,[†] Serena DeBeer,^{†,⊥} and Karl Wieghardt^{*,†}

[†]Max-Planck-Institut für Bioorganische Chemie, Stiftstrasse 34-36, D-45470 Mülheim an der Ruhr, Germany

[⊥]Department of Chemistry and Chemical Biology, Cornell University, Ithaca, New York 14853, United States

Supporting Information



ABSTRACT: The electron transfer series of complexes $[\text{Cr}(\text{bpy})_3](\text{PF}_6)_n$ ($n = 3+, 2+, 1+, 0$ (1–4)) has been synthesized and the molecular structures of 1, 2, and 3 have been determined by single-crystal X-ray crystallography; the structure of 4 has been investigated using extended X-ray absorption fine structure (EXAFS) analysis. Magnetic susceptibility measurements (4–300 K) established an $S = 3/2$ ground state for 1, an $S = 1$ ground state for 2, an $S = 1/2$ ground state for 3, and an $S = 0$ ground state for 4. The electrochemistry of this series in CH_3CN solution exhibits three reversible one-electron transfer waves. UV–vis/NIR spectra and Cr K-edge X-ray absorption spectra (XAS) are reported. The same experimental techniques have been applied for $[\text{Cr}^{\text{III}}(\text{tacn})_2]\text{Br}_3 \cdot 5\text{H}_2\text{O}$ (5) and $[\text{Cr}^{\text{II}}(\text{tacn})_2]\text{Cl}_2$ (6), which possess an $S = 3/2$ and an $S = 2$ ground state, respectively (tacn = 1,4,7-triazacyclononane, a tridentate, pure σ -donor ligand). The Cr K-edge XAS spectra of the corresponding complexes $\text{K}_4[\text{Cr}^{\text{II}}(\text{CN})_6] \cdot 10\text{H}_2\text{O}$ ($S = 1$) (7) and $\text{K}_3[\text{Cr}^{\text{III}}(\text{CN})_6]$ ($S = 3/2$) (8) have also been recorded. All complexes have been studied computationally with density functional theory (DFT) using the B3LYP functional. The molecular and electronic structures of the anionic members of the series $[\text{Cr}(\text{bpy})_3]^{1-,2-,3-}$ have also been calculated. It is unequivocally shown that all members of the electron transfer series 1–4 and $[\text{Cr}(\text{bpy})_3]^n$ ($n = 3+, 2+, 1+, 0, 1-, 2-, 3-$) possess a central Cr^{III} ion ($(t_{2g})^3$, $S = 3/2$). The three N,N' -coordinated neutral (bpy^0) ligands in the trication 1 and $[\text{Cr}^{\text{III}}(\text{bpy})_3]^{3+}$ are one-electron reduced in a stepwise fashion to localized one, two, and three π -radical anions (bpy^\bullet)¹⁻ in the dicationic, monocationic, and neutral species, respectively. Complexes 2 and $[\text{Cr}(\text{bpy})_3]^{2+}$ cannot be described as low-spin Cr^{II} species; they are in fact best described as $[\text{Cr}^{\text{III}}(\text{bpy}^\bullet)(\text{bpy}^0)_2]^{2+}$ and $[\text{Cr}^{\text{III}}(\text{bpy}^\bullet)_2(\text{bpy}^0)]^{2+}$ species. Further one-electron reductions yield one, two, and three diamagnetic (bpy^{2-})²⁻ dianions in the mono-, di-, and trianion. Thus, $[\text{Cr}^{\text{III}}(\text{bpy}^{2-})_3]^{3-}$ is a normal Werner-type Cr^{III} (!) species. In all complexes containing (bpy^\bullet)¹⁻ ligands, the ligand spins are strongly antiferromagnetically coupled to the spins of the central Cr^{III} ion (d^3 , $S_{\text{Cr}} = 3/2$) affording the observed ground states given above. Thus, all redox chemistry of $[\text{Cr}(\text{bpy})_3]^n$ complexes is ligand-based and documents that the ligand 2,2'-bipyridine is a redox noninnocent ligand; it exists in three oxidation levels in these complexes: as N,N' -coordinated neutral (bpy^0), monoanionic π -radical (bpy^\bullet)¹⁻, and diamagnetic dianionic (bpy^{2-})²⁻.

1. INTRODUCTION

Homoleptic tris(2,2'-bipyridine)metal complexes with charges ranging from 3+ to 3- have, in the past, been synthesized and in many instances been characterized by X-ray crystallography. The central metal ion may be a main group element (e.g., Al, Ga, In), any transition metal ion, or a lanthanoid ion.¹ The molecular and electronic structures of each member of an electron transfer series, such as $[\text{Cr}(\text{bpy})_3]^n$ ($n = 3+, 2+, 1+, 0, 1-, 2-, 3-$),² has, in the past 50 years, been studied by a large variety of spectroscopies, by magnetochemical and

electrochemical methods, and by X-ray crystallography of varying quality. The main difficulty in the correct assignment of the electronic structure of a given member arises from the fact that the ligands may exist in three different oxidation levels, namely as neutral (bpy^0), as π -radical monoanionic (bpy^\bullet)¹⁻, and as diamagnetic dianionic (bpy^{2-})²⁻, that is, the ligand is redox-active or redox-noninnocent. For example, the neutral,

Received: May 26, 2011

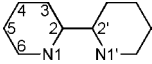
Published: November 15, 2011



diamagnetic complex $[\text{Cr}(\text{bpy})_3]^0$ can, in principle, possess any of the following electronic structures: (a) $[\text{Cr}^0(\text{bpy}^0)_3]^0$, (b) $[\text{Cr}^I(\text{bpy}^\bullet)(\text{bpy}^0)_2]^0$, (c) $[\text{Cr}^{II}(\text{bpy}^\bullet)_2(\text{bpy}^0)]^0$, and (d) $[\text{Cr}^{III}(\text{bpy}^\bullet)_3]^0$. In formulations b and c, one would encounter ligand mixed valency since two different ligand oxidation levels are present, namely, $(\text{bpy}^\bullet)^{1-}$ and $(\text{bpy}^0)^0$. Consequently, class I, II, or III behavior (Robin and Day),³ that is, localized to fully delocalized valence electrons, must be considered.

The structural differences between these three bpy oxidation levels have been assessed by X-ray structure determinations of the neutral uncoordinated ligand $(\text{bpy}^0)^0$,⁴ the salt $\text{K}(\text{bpy}^\bullet)^-(\text{en})^5$ containing the radical anion $(\text{bpy}^\bullet)^{1-}$, and $[(\text{bpy}^{2-})\{\text{Na}^+(\text{dme})\}_2]_\infty^6$ containing the diamagnetic dianion $(\text{bpy}^{2-})^{2-}$. Table 1 summarizes the average $\text{C}_{\text{py}}-\text{C}_{\text{py}}$ and C–N distances of

Table 1. Crystallographically Determined Bond Distances



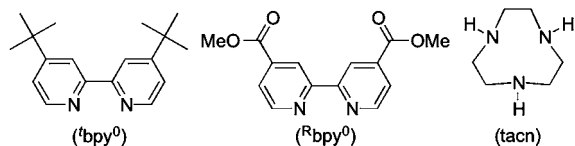
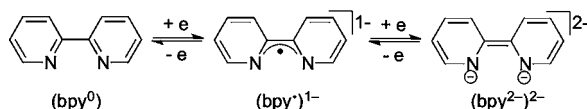
oxidation level	C2–C2', Å	C2–N1, Å	C6–N1, Å	C4–C5, Å	ref
(bpy^0)	1.490(3)	1.346(2)	1.341(2)	1.384(2)	4
$(\text{bpy}^\bullet)^{1-}$	1.431(3)	1.390(3)	1.337(2)	1.375(3)	5
$(\text{bpy}^{2-})^{2-}$	1.376(4)	1.436(5)	1.337(5)	1.365(5)	6

these species. It is clear that high-quality X-ray crystallography should, in principle, allow one to determine the oxidation level of a given N,N' -coordinated bpy ligand in a given transition metal ion. It has been repeatedly pointed out in the literature that the $\text{C}_{\text{py}}-\text{C}_{\text{py}}$ bond distance is the most significant and readily identified structural marker for the respective oxidation level: in the neutral metal-coordinated $(\text{bpy}^0)^0$ ligand, this distance is found at 1.47 ± 0.01 Å (a typical $\text{C}(\text{sp}^2)-\text{C}(\text{sp}^2)$ single bond) and in the π -radical monoanion this bond shortens to 1.43 ± 0.01 Å, whereas in the dianion it is found at 1.38 ± 0.01 Å (a $\text{C}=\text{C}$ double bond). In reality, it is not quite so simple in complexes containing three (or even four) N,N' -coordinated bpy ligands in more than one oxidation level (ligand mixed valent species) because of contributions from static disorder and the high site symmetry that may be imposed in the X-ray crystal structure determinations.

In this paper, we will establish the electronic structures of four members of the electron transfer series $[\text{Cr}(\text{bpy})_3]^n$ ($n = 3+, 2+, 1+, 0$) (complexes 1–4 in Chart 1), where use of (bpy)

Chart 1. Complexes and Ligand Abbreviations Used

$[\text{Cr}(\text{bpy})_3](\text{PF}_6)_3$ ($S = 3/2$)	1	$[\text{Cr}^{III}(\text{tacn})_2]\text{Br}_3$ ($S = 3/2$)	5
$[\text{Cr}(\text{bpy})_3](\text{PF}_6)_2$ ($S = 1$)	2	$[\text{Cr}^{II}(\text{tacn})_2]\text{Cl}_2$ ($S = 2$)	6
$[\text{Cr}(\text{bpy})_3](\text{PF}_6)$ ($S = 1/2$)	3	$\text{K}_4[\text{Cr}^{II}(\text{CN})_6]$ ($S = 1$)	7
$[\text{Cr}(\text{bpy})_3]^0$ ($S = 0$)	4	$\text{K}_3[\text{Cr}^{III}(\text{CN})_6]$ ($S = 3/2$)	8



allowed us to access higher-quality X-ray crystal structures than had been obtained using the unsubstituted (bpy) ligand (see below). The complexes containing unsubstituted (bpy) (Table 2), namely, $[\text{Cr}(\text{bpy})_3](\text{PF}_6)_3$, $[\text{Cr}(\text{bpy})_3](\text{PF}_6)_2$, $[\text{Cr}(\text{bpy})_3](\text{PF}_6)$, and $[\text{Cr}(\text{bpy})_3]^0$, have been investigated previously by X-ray crystallography^{7–9} and electronic spectroscopy¹⁰ and many contradictory electronic structures have been proposed ranging from a completely metal-centered redox series involving Cr^{III} (d^3 , $S = 3/2$), Cr^{II} (d^4 , $S = 1$), Cr^I (d^5 , $S = 1/2$), and Cr^0 (d^6 , $S = 0$) and three neutral (bpy^0) ligands in each case to a series where the reducing electrons occupy, at least partly, the π^* LUMOs of the (bpy^0) ligands. The electronic structure of the dication has been most widely described as a low-spin Cr^{II} species, namely $[\text{Cr}^{II}(\text{bpy}^0)_3](\text{PF}_6)_2$ ($S = 1$), as is evidenced by its appearance as such in multiple advanced inorganic chemistry textbooks.¹¹ It has been discussed that reduction of the dication beyond low-spin Cr^{II} cannot occur exclusively at the chromium ion, and some degree of ligand reduction must be occurring. Interestingly, although the anionic complexes $[\text{Cr}(\text{bpy})_3]^{1-, 2-, 3-}$ have been cleanly prepared and isolated as solids (Table 2)¹² and their magnetic moments have been established by magnetic susceptibility measurements, their electronic structures have not been elucidated in any detail. The original authors have proposed that $[\text{Cr}^0(\text{bpy}^0)_3]^0$ possesses a central $\text{Cr}(0)$ (d^6 , $S = 0$) and that the added electrons of the corresponding mono-, di-, and trianion would have to fill “molecular orbitals with predominantly ligand character”.¹³

Here, we will use Cr K-edge X-ray absorption spectroscopy and density functional theoretical calculations, single crystal X-ray crystallography, magneto- and electrochemistry, as well as electronic spectroscopy to establish the exact oxidation state of the central chromium ion and the corresponding oxidation level of the (bpy) ligands in complexes 1–4. In order to calibrate these results, we also investigated the complexes $[\text{Cr}(\text{tacn})_2]^{3+14}$ and $[\text{Cr}(\text{tacn})_2]^{2+}$ (complexes 5 and 6) where tacn represents the redox-inactive, pure σ -donor ligand 1,4,7-triazacyclononane. The dication in 6 possesses a central *high-spin* Cr^{II} ion (d^4 , $S = 2$). Furthermore, $[\text{Cr}^{III}(\text{CN})_6]^{3-}$ and $[\text{Cr}^{II}(\text{CN})_6]^{4-}$ (complexes 8 and 7, respectively)¹⁵ have also been studied because 7 contains a bona fide *low-spin* Cr^{II} ion (d^4 , $S = 1$). Chart 1 summarizes complexes and ligands used in this work.

With standards for genuine high- and low-spin Cr^{II} ($[\text{Cr}(\text{tacn})_2]^{2+}$ and $[\text{Cr}(\text{CN})_6]^{4-}$) in hand, we have been able to probe the electronic structure of complexes 1–4. In conjunction with (broken symmetry) DFT investigations of these compounds, we report herein that *all species in the electron-transfer series $[\text{Cr}(\text{bpy})_3]^{3+, 2+, 1+, 0}$ contain a central Cr^{III} ion, and that reduction is ligand centered in each case.* Our results call into question the assignment of all but a few species described as low-spin Cr^{II} , and suggest that low-spin Cr^{II} is a much rarer class of compounds than previously believed.¹⁶ Finally, our results show that, if high-quality X-ray crystal structures of metal complexes of bpy are available, the intraligand bond lengths may be used to assign the ligand oxidation level as $(\text{bpy}^0)^0$, $(\text{bpy}^\bullet)^{1-}$ or $(\text{bpy}^{2-})^{2-}$.¹⁷

2. EXPERIMENTAL SECTION

The following syntheses were carried out using standard Schlenk line procedures or a glovebox in the absence of water and dioxygen unless stated otherwise. The complexes 5,¹⁴ 7,¹⁵ and 8¹⁵ were prepared as described in the literature. The ligand 4,4'-di-*tert*-butyl-2,2'-bipyridine is commercially available.

Table 2. Known [Chromium(2,2'-bipyridine)₃]ⁿ Complexes and Their Proposed Electronic Structures

complex ^a	ground state	color	proposed electronic structure ^b	reference
[Cr(bpy) ₃] ³⁺	S = 3/2	yellow	Cr ^{III} (d ³)	1b
[Cr(bpy) ₃] ²⁺	S = 1	deep violet	Cr ^{II} (low-spin d ⁴)	18
[Cr(bpy) ₃] ⁺	S = 1/2	deep blue	Cr ^I (low-spin d ⁵)	18
[Cr(bpy) ₃] ⁰	S = 0	red-brown solution, black crystals	Cr ⁰ (low-spin d ⁶)	19
Li[Cr(bpy) ₃] ⁺ ·4thf	S = 1/2	red-brown solution, black-violet crystals	(?)	12
Na ₂ [Cr(bpy) ₃] ²⁻ ·7thf	S = 1	green	(?)	12
Na ₃ [Cr(bpy) ₃] ³⁻	S = 3/2	green solution, black crystals	(?)	12

^a(bpy) is used here in a generic sense; no oxidation level (neutral, monoanion, or dianion) is implied. ^bAs described by the original authors; some of these were later revised invoking participation and occupation with spin and electron density in the bpy π* orbital.

2.1. Physical Measurements. Electronic spectra of complexes were recorded with a Perkin-Elmer Lambda 19 double-beam spectrophotometer (200–2100 nm). Cyclic voltammograms were recorded with an EG&G potentiostat/galvanostat. Variable temperature (4–300 K) magnetization data were recorded in a 1 T magnetic field on a SQUID magnetometer (MPMS Quantum Design). The experimental magnetic susceptibility data were corrected for underlying diamagnetism using tabulated Pascal's constants.

2.2. Synthesis of Compounds. **2.2.1. [(^tbpy)₃Cr](PF₆)₃ (1).** [(^tbpy)₃Cr](PF₆)₂ (50 mg, 0.043 mmol) was dissolved in 2 mL of MeCN. Separately, AgPF₆ (11 mg, 0.043 mmol) was dissolved in 1 mL MeCN, and this solution was added slowly (over ~20 s) to the stirred [(^tbpy)₃Cr](PF₆)₂ solution, resulting in a change to a yellow-brown suspension. After stirring for 15 min, the MeCN was removed under vacuum to afford a brown residue. To the resulting residue was added THF, and the residue was scraped to a powder with a spatula. The THF was decanted, and the residue was washed again with THF. This process removes a dark brown impurity. The remaining solid was redissolved in MeCN and filtered through Celite. The solvent was removed under vacuum, providing pure, air-stable, bright yellow [(^tbpy)₃Cr](PF₆)₃ in 79% yield (45 mg). X-ray-quality crystals of this material were grown by vapor diffusion of Et₂O onto a concentrated MeCN solution of [(^tbpy)₃Cr](PF₆)₃. Anal. Calcd for C₃₄H₂₂N₆CrP₃F₁₈: C, 50.20; H, 5.62; N, 6.50; Cr, 4.02; P, 7.19; F, 26.47. Found: C, 50.21; H, 5.59; N, 6.49; Cr, 4.01; P, 7.18; F, 26.48.

2.2.2. [(^tbpy)₃Cr](PF₆)₂ (2). ^tbpy (503 mg, 1.87 mmol) and CrCl₂ (77 mg, 0.62 mmol) and 30 mL of degassed water were combined in a 50 mL Schlenk flask. The solution was stirred at room temperature for 20 h, during which time the color changed from light blue to deep dark blue. Five milliliters of a 0.31 M solution of NH₄PF₆ (1.55 mmol) in degassed water was added to the reaction mixture, resulting in the precipitation of [(^tbpy)₃Cr](PF₆)₂. The suspension was filtered on a Schlenk frit and the solid was washed with 50 mL degassed water. The solid was dried under vacuum, taken up in dry MeCN and filtered. Removal of the MeCN under vacuum afforded 557 mg [(^tbpy)₃Cr](PF₆)₂ (78% yield). X-ray-quality crystals of [(^tbpy)₃Cr](PF₆)₂·THF were grown by vapor diffusion of Et₂O onto a concentrated solution of [(^tbpy)₃Cr](PF₆)₂ in THF. Satisfactory elemental analysis for complexes 2, 3, and 4 could not be obtained, where in each case, the results were too low for all elements. Given the similarity of these compounds to the known analogous compounds without *tert*-butyl groups ([Cr(bpy)₃]^{3+,2+,1+}), we refer to the spectroscopic, magnetic, and X-ray crystallographic data given throughout this paper and in the Supporting Information as evidence for the purity and identity of these compounds.

2.2.3. [(^tbpy)₃Cr](PF₆) (3). [(^tbpy)₃Cr]⁰ (99 mg, 0.12 mmol) was taken up in 5 mL of THF. AgPF₆ (30 mg, 0.12 mmol) dissolved in 2 mL of THF was added dropwise (~2 drops per second) to the [(^tbpy)₃Cr]⁰ solution. The solution changed color from black to deep bluish purple. The mixture was stirred for 30 min, after which time the solvent was removed in vacuo. The solid residue was taken up in MeCN and filtered through Celite. Removal of the MeCN under vacuum afforded 113 mg of [(^tbpy)₃Cr](PF₆) (98% yield). X-ray-quality crystals of [(^tbpy)₃Cr](PF₆)·(solvate) were grown by vapor diffusion of Et₂O onto a concentrated solution of [(^tbpy)₃Cr](PF₆) in MeCN.

2.2.4. [(^tbpy)₃Cr]⁰ (4). Cr(CO)₆ (227 mg, 1.03 mmol) and ^tbpy (814 mg, 3.03 mmol) were taken up in 50 mL of mesitylene in a 100 mL Schlenk flask fitted with a reflux condenser. The system was purged with argon and heated to reflux for 24 h. After it was slowly cooled to room temperature, the crystalline product was collected on a Schlenk frit under argon and washed with 15 mL of dry degassed Et₂O. The resultant needle-like crystals were dried briefly under vacuum to afford 224 mg of black crystals (26% yield). In toluene or THF solution, the product is nearly black, but slightly red-brown.

2.2.5. [(*tacn*)₂Cr]Cl₂ (6). CrCl₂ (103 mg, 0.84 mmol) was dissolved in 3 mL of MeOH and transferred dropwise (~1 drop per second) through Celite (to remove insoluble material) to a solution of *tacn* (220 mg, 1.71 mmol) in 3 mL MeOH. The solution turned blue with concomitant formation of a small amount of insoluble yellow precipitate. After it was stirred for 15 min, this solution was filtered and cooled to -20 °C to afford X-ray-quality blue crystals of [(*tacn*)₂Cr]Cl₂·3MeOH. These crystals readily give off 3 equiv of MeOH when dried under vacuum for an hour to afford 159 mg of pure [(*tacn*)₂Cr]Cl₂ (50% yield). A second batch of product may be isolated by halving the volume of the supernatant under vacuum and transferring the solution through Celite to 8 mL of Et₂O, affording a light blue powder. The powder was collected by filtration and redissolved in minimal MeOH. This process removes any unreacted *tacn* and improves the crystallization of a second batch of product. Filtration through Celite and cooling to -20 °C afforded more crystals of [(*tacn*)₂Cr]Cl₂·3MeOH, which were dried under vacuum to afford 30 mg of a second crop of [(*tacn*)₂Cr]Cl₂ (59% yield overall). Anal. Calcd for C₁₂H₃₀N₆CrCl₂: C, 37.80; H, 7.93; N, 22.04; Cr, 13.64. Found: C, 37.64; H, 7.88; N, 21.92; Cr, 13.57.

2.3. X-ray Absorption Spectroscopy. XAS data were recorded at the Stanford Synchrotron Radiation Laboratory (SSRL) on unfocused beamline 7-3, under ring conditions of 3 GeV and 60–100 mA. A Si(220) double-crystal monochromator was used for energy selection and a Rh-coated mirror (set to an energy cutoff of 9 keV) was used for harmonic rejection in combination with 30% detuning. Internal energy calibration was performed by assigning the first inflection point of the Cr foil spectrum to 5989.0 eV. Samples were prepared by dilution in boron nitride, pressed into a pellet and sealed between 38 μm Kapton tape windows in a 1 mm aluminum spacer. Samples were maintained at 10 K during data collection using an Oxford Instruments CF1208 continuous flow liquid helium cryostat.

XAS data were measured to $k = 12 \text{ \AA}^{-1}$, the data range is truncated due to the presence of monochromator glitches at higher k . The data were calibrated and averaged using EXAFSPAK.²⁰ Pre-edge subtraction and splining were carried out using PYSPLINE.²¹ A three-region cubic spline of order 2, 3, 3 was used to model the smooth background above the edge. Normalization of the data was achieved by subtracting the spline and normalizing the postedge region to 1. The resultant EXAFS was k^3 -weighted to enhance the impact of high- k data.

Theoretical EXAFS signals $\chi(k)$ were calculated using FEFF (version 7.0)^{22,23} and fit to the data using EXAFSPAK.²⁰ The nonstructural parameter E_0 was also allowed to vary but was restricted to a common value for every component in a given fit. The structural parameters varied during the refinements were the bond distance (R)

and the bond variance (σ^2). The σ^2 is related to the Debye–Waller factor, which is a measure of thermal vibration and to static disorder of the absorbers/scatterers. Coordination numbers were systematically varied in the course of the analysis, but they were not allowed to vary within a given fit.

2.4. Calculations. All DFT calculations were performed with the ORCA program.^{23b} The complexes were geometry optimized using the B3LYP functional.^{24,25} The all-electron basis sets were those reported by the Ahlrichs group.^{26,27} Triple- ζ -quality basis sets with one set of polarization functions (TZVP) were used for the Cr metal and the nitrogen atoms coordinated to it. The remaining atoms were described by slightly smaller polarized split-valence SV(P) basis sets that are double- ζ -quality in the valence region and contain a polarizing set of d functions on the non-hydrogen atoms.²⁷ Auxiliary basis sets used to expand the electron density in the calculations were chosen to match the orbital basis. Electronic energies and properties were calculated at the optimized geometries using the B3LYP functional.^{24,25} In this case the same basis sets were used. The self-consistent field calculations were tightly converged (1×10^{-8} E_h in energy, 1×10^{-7} E_h in the density charge, and 1×10^{-7} in the maximum element of the DIIS²⁸ error vector). The geometry search for all complexes was carried out in redundant internal coordinates without imposing geometry constraints. Corresponding²⁹ and quasi-restricted³⁰ orbitals and density plots were obtained using Molekel.³¹ For the charged species $[\text{Cr}(\text{bpy})_3]^{3+,2+,1+,1-,2-,3-}$, geometry optimizations were carried out normally as well as by applying the conductor-like screening model (COSMO)³² to model solvation in water (dielectric constant (ϵ) = 80.4, refractive index = 1.33).³³ We used the broken symmetry (BS) approach to describe our computational results for **2**, **3**, **4**, and the anions $[\text{Cr}(\text{bpy})_3]^n$ ($n = 1-, 2-$).³⁴ We adopted the following notation: the given system was divided into two fragments. The notation BS(m,n) refers then to a broken symmetry state with m unpaired α -spin electrons essentially on fragment 1 and n unpaired β -spin electrons localized on fragment 2. In each case, fragments 1 and 2 correspond to the metal and the ligands, respectively. In this notation the standard high-spin, open-shell solution is written as BS($m + n, 0$). The BS(m,n) notation refers to the initial guess to the wave function. The variational process does, however, have the freedom to converge to a solution of the form BS($m - n, 0$) in which effectively the n β -spin electrons pair up with $n < m$ α -spin electrons on the partner fragment. Such a solution is then a standard $M_s \approx (m - n)/2$ spin-unrestricted Kohn–Sham solution. As explained elsewhere,²⁹ the nature of the solution is investigated from the corresponding orbital transformation (COT) which, from the corresponding orbital overlaps, displays whether the system should be described as a spin-coupled or a closed-shell solution.

Time-dependent (TD-DFT) calculations of the Cr metal K-pre-edges were conducted as previously described.^{35,36} For all complexes, the B3LYP functional was used in conjunction with the fully uncontracted CP(PPP) basis set for the metal,³⁷ TZVP for the nitrogen atoms and SV(P) for the remaining atoms for a single-point, spin unrestricted ground state DFT calculation starting from the optimized coordinates. TD-DFT calculations³⁸ were then performed allowing only for transitions from the metal 1s orbital.^{36,38} The absolute calculated transition energies are consistently underestimated because of the shortcomings in the ability of DFT to model potentials near the nucleus. This results in the deep 1s core orbitals being too high in energy relative to the valence, thus requiring a constant shift for a given absorber. It was established that a shift of 125.79 eV for Cr K-edge is required for this regime of basis sets and applied to the transition energies. Plots were obtained using “orca_mapspc” with a line broadening of 1.0 eV for Cr K-edges. Despite the inherent restrictions in describing open-shell systems with a single determinantal reference wave function, we have found that this method is quite effective at predicting the energy and relative intensities originating from the Cr 1s orbital for complexes **1–8**.

3. RESULTS

3.1. Synthesis and Characterization of Compounds.

Synthetic access to purple $[\text{Cr}(\text{bpy})_3](\text{PF}_6)_2$ (**2**) is achieved by combining the appropriate 3:1 stoichiometry of ligand and CrCl_2 in degassed water. Addition of NH_4PF_6 precipitates the desired dicationic hexafluorophosphate salt, which was isolated in pure crystalline form by vapor diffusion. Air-stable, yellow $[\text{Cr}(\text{bpy})_3](\text{PF}_6)_3$ (**1**) is most conveniently formed by oxidation of **2** with AgPF_6 . Synthetic access to deep blue-purple $[\text{Cr}(\text{bpy})_3](\text{PF}_6)_3$ (**3**) is obtained by oxidation of black $[\text{Cr}(\text{bpy})_3]^0$ (**4**) with one equivalent of AgPF_6 . **4** was prepared by combining $\text{Cr}(\text{CO})_6$ with three equivalents of (bpy^0) in mesitylene and heating the solution to reflux. $[(\text{tacn})_2\text{Cr}]\text{Cl}_2$ (**6**) was prepared by addition of two equivalents of tacn to CrCl_2 in CH_3OH under the rigorous exclusion of air and was isolated as the crystalline methanol solvate complex from a cold methanol solution. $[\text{Cr}(\text{tacn})_2]\text{Br}_3$ ¹⁴ and $\text{K}_4[\text{Cr}(\text{CN})_6]$ ¹⁵ were prepared according to the literature.

From temperature dependent (4–300 K) magnetic susceptibility measurements of solid samples of complexes **1–3**, temperature-independent (40–300 K) magnetic moments of $3.8 \mu_B$ for **1**, $3.0 \mu_B$ for **2**, and $1.8 \mu_B$ for **3** (Figure 1) have been

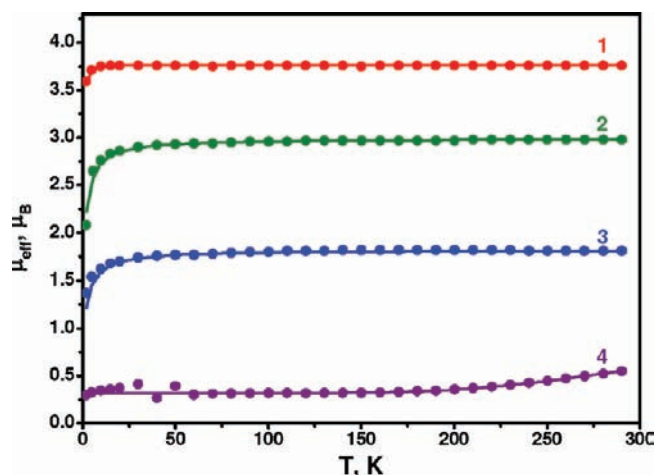


Figure 1. Temperature dependence of the magnetic moments of **1**, **2**, and **3**. Solid lines represent best fits of the experimental data (see Supporting Information).

established, indicating an $S = 3/2$ ground state for **1**, an $S = 1$ ground state for **2**, and an $S = 1/2$ ground state for **3**. The same results have been reported for the unsubstituted $[\text{Cr}(\text{bpy})_3]^{3+,2+,1+}$ series.¹ Figure 2 shows the temperature dependence of the magnetic moment of the neutral complex **4** and a fit of the data using the Heisenberg–Dirac–van Vleck (HDvV) spin Hamiltonian operator, eq 1, for the spin exchange coupling between the central Cr^{III} ion (d^3 , $S_{\text{Cr}} = 3/2$) and three ligand π -radical anions ($S_{\text{rad}} = 1/2$).

$$\hat{H} = -2J \sum_i S_{\text{Cr}} \times S_i (S_{\text{Cr}} = 3/2; S_i = 1/2; i = 1, 2, 3) \quad (1)$$

The large exchange coupling constant J of $-477 \pm 20 \text{ cm}^{-1}$ indicates a strong antiferromagnetic coupling between three ligand radicals $(\text{bpy}^\bullet)^{1-}$ and the central Cr^{III} ion. These data indicate that, although **4** possesses an $S = 0$ ground state, its electronic structure cannot be described by a closed-shell model such as $[\text{Cr}^{\text{VI}}(\text{bpy}^{2-})_3]^0$ or $[\text{Cr}^0(\text{bpy}^0)_3]^0$. Very similar results have been reported in 1972 for $[\text{Cr}(\text{bpy})_3]^0$.³⁹

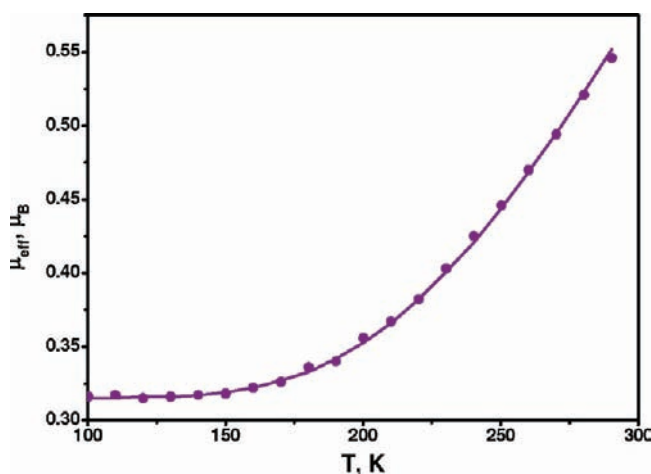


Figure 2. Temperature dependence of the magnetic moment of **4** (100–300 K). The solid line represents a best fit to the data according to eq 1 with $J = -477 \text{ cm}^{-1}$ and $g = 2.00$, and a paramagnetic impurity of 0.7% ($S = 3/2$).

Complexes **5** and **6** display temperature-independent magnetic moments of $3.8 \mu_B$ and $4.9 \mu_B$ indicative of an $S = 3/2$ and an $S = 2$ ground state, respectively (see Supporting Information). Thus, **6** contains a genuine high-spin Cr^{II} (d^4) ion.

For complexes **7** and **8**, ground states of $S = 1^{5,40}$ and $S = 3/2^{41}$ respectively, have been determined previously (see Supporting Information). **7** contains a central low-spin Cr^{II} (d^4) ion.

The X-band EPR spectrum of **3** ($S = 1/2$) has been recorded in toluene solution at 295 K and is shown in the Supporting Information. From a simulation the following parameters have been established: $g_{\text{iso}} = 1.99906$; $A(^{53}\text{Cr}) = 20.43 \times 10^{-4} \text{ cm}^{-1}$, and $A(^{14}\text{N}) = 2.74 \times 10^{-4} \text{ cm}^{-1}$. These data are nearly identical to those reported by König in 1964 for $[\text{Cr}(\text{bpy})_3]^{1+}$ ($g_{\text{iso}} = 1.9973$; $A(^{53}\text{Cr}) = 21.8 \times 10^{-4} \text{ cm}^{-1}$, and $A(^{14}\text{N}) = 3.05 \times 10^{-4} \text{ cm}^{-1}$).⁵⁴ These large ^{53}Cr hyperfine couplings in both complexes clearly demonstrate that the unpaired electron resides in a d-orbital (in O_h symmetry in a t_{2g} orbital) in each case. König⁵⁴ has proposed a $[\text{Cr}^{\text{I}}(\text{bpy}^0)_3]^{1+}$ (low-spin d^5) electronic structure. We show here that a structure as in $[\text{Cr}^{\text{III}}(\text{bpy}^\bullet)_2(\text{bpy}^0)]^{1+}$ is the more appropriate description but it is not possible to unambiguously discern between these two possibilities by the X-band EPR spectra.

3.2. Electronic Absorption Spectra. The electronic spectra of $(\text{bpy}^\bullet)^{1-}$ and $(\text{bpy}^{2-})^{2-}$ in dioxane solution have been measured and interpreted by König and Kremer in 1970.⁴² They reported three intense ($\epsilon \approx 10^4 \text{ M}^{-1} \text{ cm}^{-1}$) bands each with a characteristic vibrational structure at ~ 820 , 530 , and 385 nm for the π -radical anion $(\text{bpy}^\bullet)^{1-}$, and two intense bands at ~ 610 and 373 nm for $(\text{bpy}^{2-})^{2-}$.

The electronic spectra of $[\text{Cr}(\text{bpy})_3]^{n+}$ ($n = 0-3$) are shown in Figure 3. They are very similar to those reported for $[\text{Cr}(\text{bpy})_3]^{n+}$ ($n = 0-3$).¹⁰ The results reveal that the spectra of species $n = 0-2$ show similar transitions in the visible and near-infrared (NIR), the intensities of which increase incrementally with decreasing n (increasing reduction). Keeping in mind the spectrum of uncoordinated $(\text{bpy}^\bullet)^{1-}$, it is possible to assign two bands with a center of gravity at $\sim 1100 \text{ nm}$ and $\sim 520 \text{ nm}$ as transitions arising from one $(\text{bpy}^\bullet)^{1-}$ in $[\text{Cr}(\text{bpy})_3]^{2+}$, two in $[\text{Cr}(\text{bpy})_3]^{1+}$, or three in $[\text{Cr}(\text{bpy})_3]^{0}$. These similarities have been noted previously.^{10a} The yellow complexes **1** and

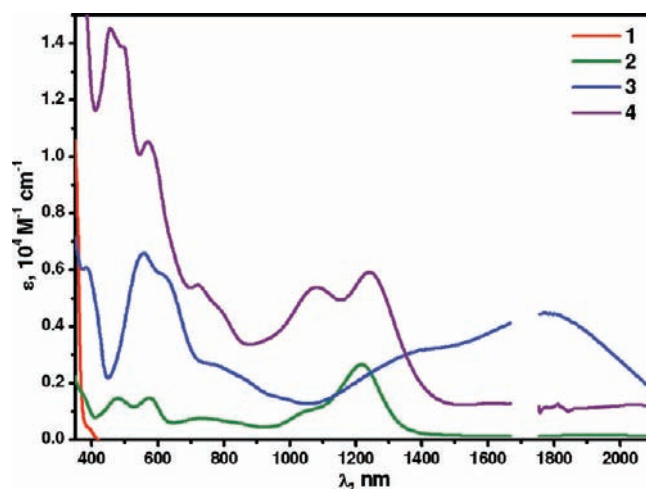


Figure 3. Electronic spectra of complexes **1–4** in solution (**1** in acetonitrile; **2**, **3**, and **4** in tetrahydrofuran) at 22°C .

$[\text{Cr}(\text{bpy})_3]^{3+}$ do not exhibit these bands and their electronic structures have been described as $[\text{Cr}^{\text{III}}(\text{bpy}^0)_3]^{3+}$, where $d-d$ transitions are observed in the visible only.^{7b} The spectrum of **3** exhibits an additional intense transition at 1800 nm that is tentatively assigned as a ligand-to-ligand intervalence charge transfer band.

3.3. Crystal Structure Determinations. The crystal structures of **1**, **2**, **3**, **5**, and **6** have been determined by single-crystal X-ray crystallography at cryogenic ($100(2) \text{ K}$) temperature. The trication in **1** (Figure 4a) possesses a crystallographic C_2 -axis. There are three equivalent neutral, N,N' -coordinated (bpy^0) ligands and three well separated PF_6^- anions. The geometric details of the three bpy ligands (Table 3) clearly define their oxidation level as (bpy^0) as demonstrated by the long $C_{\text{py}}-C_{\text{py}}$ distance at $1.479 \pm 0.006 \text{ \AA}$ and the short $C-N$ distances at $1.355 \pm 0.005 \text{ \AA}$. This result is very similar to that reported for $[\text{Cr}^{\text{III}}(\text{bpy})_3](\text{PF}_6)_3$.^{7,8} The average $\text{Cr}-\text{N}$ distances are equivalent within the 3σ limit at an average distance of 2.038 \AA .

The X-ray crystal structure of $[\text{Cr}(\text{bpy})_3](\text{PF}_6)_2$ has also been reported;⁸ however, a crystallographic C_3 -axis precluded the possibility of observing bond-length changes consistent with a localized, one-electron reduction of one of the three bpy ligands. Because of the presence of a crystallographic C_3 -axis, a quinoidal distortion associated with a single one-electron-reduced bpy ligand, if present, would be averaged across all three bpy ligands. Only a high-quality crystal structure, wherein each ligand is crystallographically independent, would distinguish between a localized, singly reduced ligand and either a delocalized singly reduced tris- bpy spin system or a true low-spin Cr^{II} . We have utilized bpy ligands with the hope of obtaining lower-symmetry crystal structures than obtained with bpy . Luckily, our crystal structure of $[\text{Cr}(\text{bpy})_3](\text{PF}_6)_2$ (**2**) does not possess a crystallographic C_2 - or C_3 -axis passing through the Cr atom, resulting in three crystallographically independent bpy ligands coordinated to Cr (Figure 4 and Table 3). Metric parameters in the dication reveal that two bpy ligands are nearly identical (bpy_1 and bpy_2 in Table 3), whereas the third bpy ligand (bpy_3 in Table 3) has undergone a statistically significant quinoidal distortion. This distortion is largest in the $C_{\text{py}}-C_{\text{py}}$ bond lengths connecting the two pyridyl units of bpy , and is also observed in the $C_{\text{py}}-N$ bond lengths (Table 3). The localized quinoidal distortion of one bpy ligand in **2** is

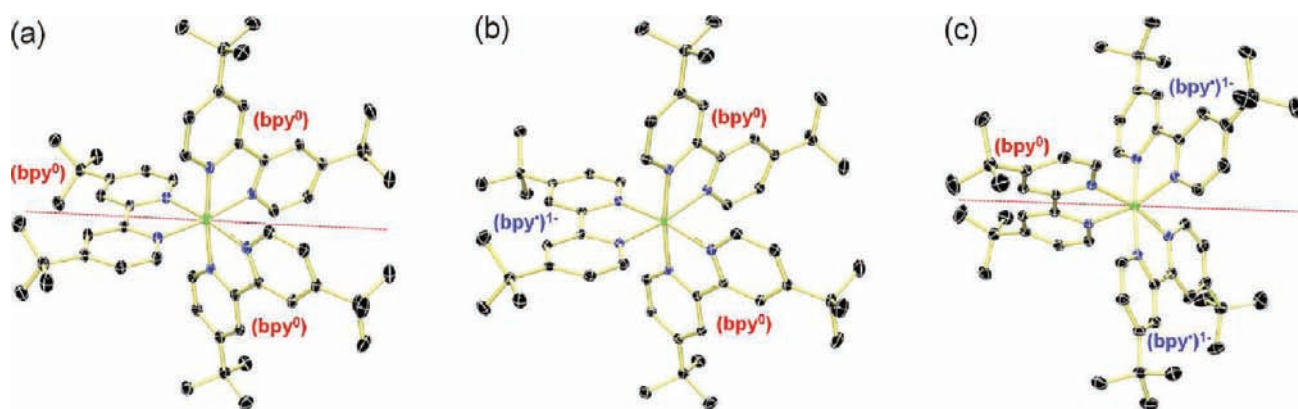


Figure 4. Structures of (a) the trication in crystals of **1**, (b) the dication in **2**, and (c) the monocation in **3**. The dotted lines in panels a and c represent a crystallographic C_2 -axis.

Table 3. Bond Lengths (Å) Observed in the Solid-State Molecular Structures of Complexes **1–3**

bond	1		2			3	
	^t bpy-1 ^a	^t bpy-2 ^a	^t bpy-1	^t bpy-2	^t bpy-3	^t bpy-1 ^a	^t bpy-2 ^a
Cr–N1	2.0413(11)	2.0257(11)	2.0613(14)	2.0671(14)	1.9942(14)	2.0122(16)	2.0365(15)
Cr–N2	2.0476(11)		2.0693(14)	2.0588(14)	1.9884(14)	1.9972(15)	
N1–C1	1.3543(16)	1.3595(15)	1.361(2)	1.359(2)	1.373(2)	1.373(2)	1.362(2)
N2–C2	1.3566(16)		1.357(2)	1.358(2)	1.372(2)	1.375(3)	
C1–C2	1.4787(16)	1.479(2)	1.473(2)	1.475(2)	1.452(2)	1.437(2)	1.460(3)

^aThe crystallographic C_2 -axis results in two independent ^tbpy ligands, in which there is one ^tbpy-1 ligand and one-half ^tbpy-2 ligand in the unit cell.

smaller in magnitude than observed in some other complexes containing only one (^tbpy)^{1–} ligand (see below), but is nonetheless consistent with a localized or partially localized ^tbpy-centered radical anion. The largest structural difference between the nearly identical neutral (^tbpy)⁰ pair and the quinoidally distorted (^tbpy)^{1–} are observed in the Cr–N bond lengths, where the differences are well outside of the 3σ limit (≥ 0.056 Å). This is considered to reflect a purely electrostatic effect: the Cr–N distance is slightly longer (weaker) when a neutral (^tbpy)⁰ is bound than when a monoanionic π -radical is coordinated to a central tricationic chromium(III) ion. Therefore, the crystallographic data of **2** and its UV–vis/NIR absorption spectrum are inconsistent with the long-held view that $[\text{Cr}(\text{bpy})_3]^{2+}$ is best described as low-spin Cr^{II} .¹¹

A localized reduction of ^tbpy is also observed in our crystal structure of $[\text{Cr}(\text{bpy})_3](\text{PF}_6)$ (**3**), which possesses a single C_2 -axis passing through the chromium center. In this species, the two equivalent ligands have undergone a quinoidal distortion, while the metric parameters of the third ligand are consistent with a neutral oxidation level (Table 3 and Figure 4). The assignment as $[\text{Cr}^{\text{III}}(\text{bpy})_2(\text{bpy}^{\bullet})]^{1+}$ is again supported by the observed Cr–N bond distances: four equivalent shorter bonds at 2.005 Å are present and are indicative of two (^tbpy)^{1–}; two longer bonds at 2.036 Å represent a single neutral (^tbpy)⁰ ligand. As with $[\text{Cr}(\text{bpy})_3]^{2+}$, the known crystal structure of $[\text{Cr}(\text{bpy})_3]^{1+}$ possesses a crystallographic C_3 -axis passing through the chromium center, averaging the bond lengths of all three ligands,⁸ whereas the ^tBu groups present in our structure provide a lower-symmetry unit cell in which localized quinoidal distortions are observed.

Taking the crystallographically determined average Cr–N distances of 2.038 Å in **1**, 2.040 Å in **2**, and 2.015 Å in **3**, it is evident that a change of the oxidation state of the central metal ion in this series is probably not manifest, since a reduction of the central metal ion would result in an increase of the Cr–N bond.

Despite many attempts, we could not obtain X-ray-quality crystals of neutral **4**. Therefore, we have determined its structure by using EXAFS (extended X-ray absorption fine structure) of a powdered sample of **4** (see below). The structure of neutral $[\text{Cr}(\text{bpy})_3]^0$ has been reported in part but not completed due to twinning problems.⁷

The saturated macrocycle 1,4,7-triazacyclononane is a tridentate pure σ -donor with no π -acceptor capability. Many octahedral bis(1,4,7-triazacyclononane)metal complexes have been synthesized and structurally characterized.⁴³ Here, we report the structures of $[\text{Cr}^{\text{III}}(\text{tacn})_2]\text{Br}_3 \cdot 5\text{H}_2\text{O}$ (**5**) and its one-electron reduced analog $[\text{Cr}^{\text{II}}(\text{tacn})_2]\text{Cl}_2 \cdot 3\text{CH}_3\text{OH}$ (**6**), where the former possesses a central Cr^{III} ion ($S = 3/2$) and the latter is a high-spin Cr^{II} ($S = 2$) species. Figure 5 displays the structures: in **5**, the six Cr–N distances are equivalent at 2.073(1) Å, whereas in **6**, these bonds are inequivalent: two long axial Cr–N bonds at 2.4193(7) and 2.3871(7) Å and four shorter equatorial distances at 2.1340(6), 2.1508(6), 2.1886(7), and 2.1610(6) Å indicate the presence of a Jahn–Teller Cr^{II} ion (d^4 , $S = 2$) in an elongated octahedral environment of six secondary amine nitrogen donor atoms. Thus, **6** is a high-spin Cr^{II} species.

The crystal structures of $\text{Na}_4[\text{Cr}(\text{CN})_6] \cdot 10\text{H}_2\text{O}$ (**7**)⁴⁴ and $\text{K}_3[\text{Cr}^{\text{III}}(\text{CN})_6]$ (**8**)⁴⁵ have been reported. Complex **7** represents a genuine low-spin Cr^{II} species (d^4 , $S = 1$) whereas **8** is a typical Cr^{III} complex ($S = 3/2$). The average Cr–C distance in

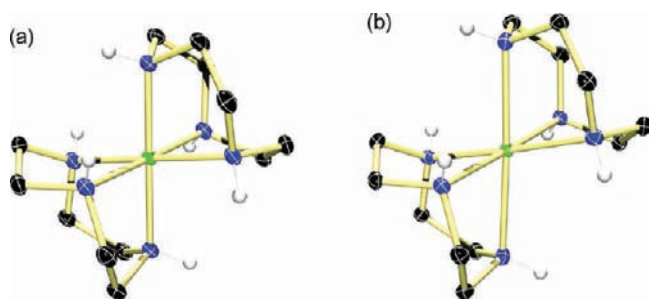


Figure 5. Solid-state molecular structure of the cations in (a) $[\text{Cr}^{\text{III}}(\text{tacn})_2]\text{Br}_3 \cdot 5\text{H}_2\text{O}$ (**5**) and (b) in $[\text{Cr}^{\text{II}}(\text{tacn})_2]\text{Cl}_2 \cdot 3\text{CH}_3\text{OH}$ (**6**).

7 is 2.053(4) Å, whereas that in **8** is 2.077(10) Å. Cyanide is a strong π -acceptor ligand and, therefore, the $\text{Cr}^{\text{III}}\text{--C}$ bonds in **8** are longer than those in the corresponding complex **7** (stronger π -backdonation).

3.4. Electrochemistry. The electrochemistry of complexes $[\text{Cr}(\text{bpy})_3]^{n+}$ ($n = 3, 2, 1, 0$) dissolved in various solvents has, in the past, been repeatedly investigated by polarographic and cyclic voltammetric methods.^{46–49} It has been established that, in the potential range from 0 to -3.0 V vs Fc^+/Fc , there are six reversible one-electron transfer processes observed. Thus, seven distinct species are stable in solution under these conditions: $[\text{Cr}(\text{bpy})_3]^n$ ($n = 3+, 2+, 1+, 0, 1-, 2-, 3-$), all of which have been isolated in the past as solid materials (Table 2). It has been noted that the spacing between the first three waves ($\Delta(E(3+/2+)) - E(2+/1+)$) and $\Delta(E(2+/1+) - E(1+/0))$) is constant at approximately -0.54 V, whereas for the next three waves this difference is smaller at ~ -0.25 V. These data, along with the changes of redox potentials observed upon substitution of the bpy-backbone hydrogens, have been interpreted in the following three ways: (1) one-electron reduction of $[\text{Cr}^{\text{III}}(\text{bpy}^0)_3]^{3+}$ is a metal-centered process (reduction to low-spin Cr^{II}), whereas subsequent reductions occur into primarily ligand-centered orbitals;^{46a} (2) the first three one-electron reductions of $[\text{Cr}^{\text{III}}(\text{bpy}^0)_3]^{3+}$ occur into metal-centered orbitals, whereas subsequent one-electron reduction may be metal-^{46b} or ligand-centered;^{47b} and (3) the localization of the electrons added upon consecutive one-electron reductions of $[\text{Cr}^{\text{II}}(\text{bpy})_3]^{2+}$ is ambiguous.^{47a} In a recent report, six reversible one-electron reductions of $[\text{Cr}^{\text{III}}(\text{R}^{\text{bpy}})_3]^{3+}$ (R^{bpy} is 4,4'-di(carboxymethyl)-2,2'-dipyridyl) were observed by cyclic voltammetry that were shifted by $\sim +45$ mV (for the first three reductions) and $\sim +70$ mV (for the last three reductions) compared to the same reductions of the unsubstituted species $[\text{Cr}^{\text{III}}(\text{bpy}^0)_3]^{3+}$. The authors proposed that the reducing electrons might be primarily localized in ligand-centered orbitals.⁴⁸ In this latter interpretation of $[\text{Cr}^{\text{III}}(\text{bpy})_3]^{3+}$ species, a stepwise one-electron reduction of three neutral (bpy^0) ligands in the trication $[\text{Cr}(\text{bpy})_3]^{3+}$ to three localized ($\text{bpy}^{\bullet-}$)¹⁻ radical monoanions in the neutral complex $[\text{Cr}(\text{bpy})_3]^0$ occurs. Further reductions to the mono-, di-, and trianion may then involve the stepwise transformation of three ($\text{bpy}^{\bullet-}$)¹⁻ ligands to the corresponding N,N' -coordinated dianion (bpy^{2-})²⁻.^{46–49} Note that in this interpretation, the central chromium ion invariably possesses a +III oxidation state.

Figure 6 displays the CV of complex **1** in acetonitrile (0.10 M $[\text{N}(\text{nBu})_4](\text{PF}_6)$) at 22 °C. In the potential range from 0 to -2.0 V vs Fc^+/Fc , three fully reversible one-electron transfer waves are observed indicating that the following four species

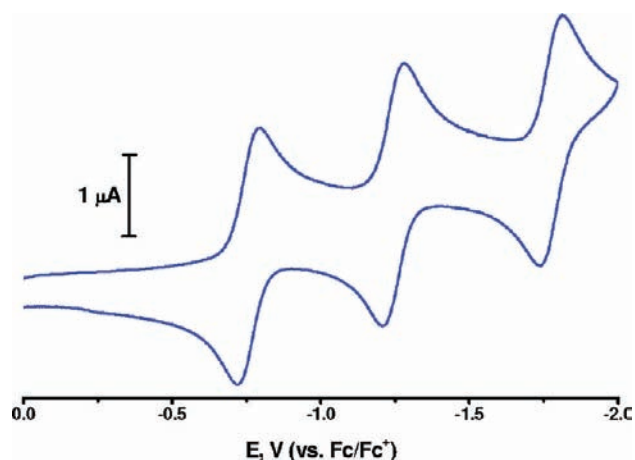


Figure 6. Cyclic voltammogram of **1** in CH_3CN solution (0.10 M $[\text{N}(\text{n-Bu})_4](\text{PF}_6)$ supporting electrolyte) at 22 °C (glassy carbon working electrode, scan rate 100 mV s^{-1} ; potentials are referenced vs the ferrocene/ferrocenium couple (Fc/Fc^+)).

$[\text{Cr}(\text{bpy})_3]^n$ ($n = 3+, 2+, 1+, 0$) are stable in solution; at more negative potentials, no reversible reduction waves are observed, indicating that the anions are not stable to these conditions. The individual $E_{1/2}$ values for the $3+/2+$, $2+/1+$, $1+/0$ couples (Table 4) are observed at slightly more negative potentials than those of the unsubstituted $[\text{Cr}(\text{bpy})_3]^{n+}$ series (shifts of -0.16 , -0.13 , -0.09 V are observed, respectively). The large effect of bpy substitution on redox potential (the 4,4'-di(carboxymethyl)-2,2'-bipyridine is more electron poor and the corresponding 4,4'-di-*tert*-butyl analog is more electron rich than bpy itself) may indicate that these redox processes are ligand centered.^{46,47,49}

3.5. Chromium K-edge X-ray Absorption Spectroscopy. The above data provide strong evidence for consecutive one-electron reductions of $[\text{Cr}(\text{bpy})_3]^{3+}$ occurring into localized ligand-centered orbitals. This would require the oxidation state of the chromium center to remain in a trivalent state throughout this electron transfer series. We sought to probe the valency of the chromium center directly using chromium K-edge X-ray absorption spectroscopy (XAS). This method is conveniently element specific and excitation occurs from the chromium 1s orbital into unoccupied orbitals. The lowest-energy transitions (1s to 3d) occurring in the pre-edge region of an XAS spectrum are expected to be quite sensitive to the oxidation state of the chromium. To confirm this notion, we have obtained the XAS spectra of two sets of reference compounds: (1) $[\text{Cr}^{\text{III}}(\text{tacn})_2]^{3+}$ (**5**, $S = 3/2$) and $[\text{Cr}^{\text{II}}(\text{tacn})_2]^{2+}$ (**6**, $S = 2$), our standard for high-spin Cr^{II} ; and (2) $[\text{Cr}^{\text{III}}(\text{CN})_6]^{3-}$ (**8**, $S = 3/2$) and $[\text{Cr}^{\text{II}}(\text{CN})_6]^{4-}$ (**7**, $S = 1$), our standard for low-spin Cr^{II} (Figure 7). As expected, the pre-edge transitions appear at lower energy for the divalent (**6**) than for the trivalent (**5**) Cr species, with a shift of 1.7 eV occurring upon oxidation. For the low-spin $\text{Cr}(\text{III})/\text{Cr}(\text{II})$ couple in $[\text{Cr}(\text{CN})_6]^{3-/4-}$ the trend in pre-edge energies is the same; however, the increase in energy upon oxidation is smaller (1.1 eV). In any case, it is clear that oxidation state, as well as the coupled changes in the ligand field, will contribute to the observed pre-edge energy. The position of the rising edge is also expected to shift to lower energy upon metal-centered reduction, and this is indeed observed for both sets of compounds. However, due to the large number of peaks superimposed on the rising edge (which are more ambiguous in

Table 4. Ground State Reduction Potentials for Tris(bipyridine)chromium Complexes (Potentials Are Referenced versus the Ferrocenium/Ferrocene Couple, Fc⁺/Fc)

	$E_{1/2}$, V						ref
	3+/2+ couple	2+/1+ couple	1+/0 couple	0/1- couple	1-/2- couple	2-/3- couple	
[Cr(bpy) ₃] ⁿ	-0.63	-1.15	-1.72	-2.34	-2.67	-2.90	27
[Cr(^t bpy) ₃] ^{n^a}	-0.79	-1.28	-1.81				this work
[Cr(^R bpy) ₃] ^{n^a}	-0.26	-0.68	-1.21	-1.74	-1.93	-2.10	48

^aR = CO₂Me and *t* = tertiary butyl in the 4- and 4'-positions of the 2,2'-bipyridine ligands.

their formal assignments and likely involve transitions with significant ^tbpy π* character, 1s to 4p transitions, as well as transitions to higher-energy Rydberg states), we rely here on the position of the lowest-energy pre-edge transition as a probe of the chromium oxidation state, as this can also be well correlated to the computational results described below. We note, however, that in the Cr(III)/Cr(II) couples in [Cr(CN)₆]^{3-/4-} and [(tacn)₂Cr]^{3+/2+}, the main edge and all features superimposed on the rising edge also shift to higher energy upon oxidation from Cr(II) to Cr(III), consistent with metal-based redox processes in these couples. We also note that the position of the lowest-energy pre-edge feature in the Cr(III) complexes 5 and 8 is nearly identical (5990.4 and 5990.2 eV, respectively), suggesting that the energy of this transition in Cr(III) complexes may not be particularly ligand dependent. As further evidence that the position of the lowest-energy pre-edge feature is largely unaffected by the nature of the ligands in octahedral Cr(III) complexes, we have compiled the data shown in Table 5, which includes compounds from related studies on Cr(III) species. The position of the lowest-energy pre-edge feature across this series of Cr(III) complexes ranges from

5990.2 to 5990.7 eV (c.f. the larger changes observed upon metal-centered reduction of 1.1 (8) and 1.7 eV (5)) despite the fact that this list includes ligands which are pure σ-donors, π-donors, and π-acceptors. Given the combined data on octahedral Cr(II) and Cr(III) complexes described above, we conclude that the energy of the first pre-edge feature in octahedral chromium complexes is a reliable marker for chromium oxidation state assignments.

With a knowledge of the effect of metal oxidation state on the position of the lowest-energy pre-edge transition in chromium K-edge XAS, we examined the XAS spectra of all species in the electron transfer series [Cr(^tbpy)₃]ⁿ (n = 3+, 2+, 1+, 0). In contrast to the data shown in Figure 7, here the rising edges are all quite similar and reflect a similar Z_{eff} on the metal.

Table 5. Comparison of Calculated and Experimentally-Determined Cr K-Edge Energies (eV) of Complexes

complex	calcd ^a	exp	ref
<i>trans</i> -[Cr ^{III} Cl ₂ (OH ₂) ₄]Cl		5990.6	51
		5992.7	
[Cr ^{III} (^{3,6} L _{sq} [•]) ₃] ^{0b}		5990.7	51
		5992.8	
[Cr ^{III} (^{3,6} t [•] L _{sq}) ₂ (^{3,6} L _{cat})] ^{1- b}		5990.7	51
		5992.9	
[Cr ^{III} (mnt) ₃] ^{3-b}		5990.3	52
		5992.4	
1	5990.4	5990.4	this work
	5991.7	5993.1	
	5994.6		
2	5990.1	~5990.4	this work
	5991.3		
	5993.0		
3	5990.5	5990.4	this work
	5991.5		
	5993.0		
4	5990.5	5990.4	this work
	5991.6		
	5993.3		
5	5990.4	5990.4	this work
	5991.6	5992.7	
		5997.7	
6	5988.7	5988.4	this work
	5990.0–5990.7	5989.3	
		5991.0	
7	5989.2	5989.1	this work
	5991.0	5991.0	
8	5990.3	5990.2	this work
	5992.1	5990.9	

^aAll calculated transitions are increased by 125.79 eV. ^b(^{3,6}L_{sq}[•]) represents 3,6-di-*tert*-butylbenzosemiquinonate (1-) and (^{3,6}L_{cat}) is its one-electron reduced dianion; (mnt)²⁻ is maleonitrile dithiolate (2-).

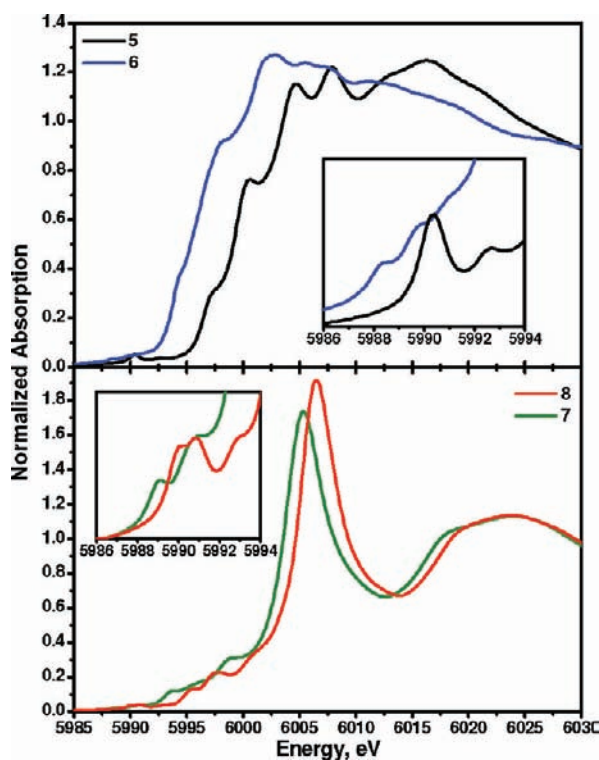


Figure 7. Normalized Cr K-edge X-ray absorption spectra of the pairs [(tacn)₂Cr^{III}]Br₃ (5) and [(tacn)₂Cr^{II}]Cl₂ (6) (top) and K₃[(CN)₆Cr^{III}] (8) and K₄[(CN)₆Cr^{II}] (7) (bottom). The insets show expansions of the lowest-energy transitions in the pre-edge region.

In addition, the lowest-energy pre-edge transition of each species is energetically indistinguishable at 5990.4 eV (Table 5 and Figure 8). These results are strong evidence that all species

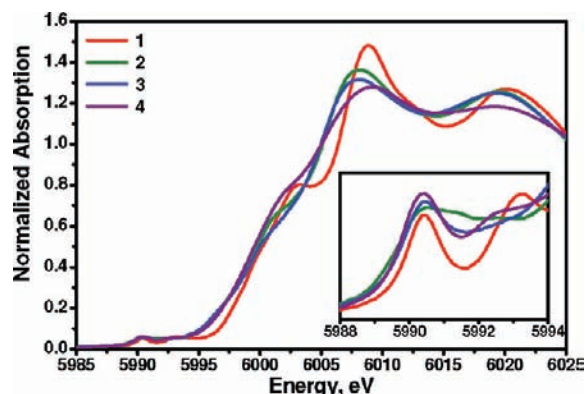


Figure 8. Cr K-edge X-ray absorption spectra of the members of the electron transfer series $[\text{Cr}(\text{tbpy})_3]^n$ ($n = 3+$ (1), $2+$ (2), $1+$ (3) and 0 (4)). The inset shows an expansion of the first transitions in the pre-edge region.

in this electron transfer series contain a Cr-center in the same oxidation state. As $[\text{Cr}(\text{tbpy})_3]^{3+}$ is unambiguously assigned as high-spin Cr^{III} , we conclude that all species of the electron transfer series $[\text{Cr}(\text{tbpy})_3]^n$ ($n = 3+, 2+, 1+, 0$) contain a high-spin Cr^{III} center. In each case, the one-electron reduction is, therefore, ligand centered.

We also note that the energy of the lowest Cr K-pre-edge peak in $[\text{Cr}^{\text{III}}(\text{tacn})_2]^{3+}$ at 5990.4 eV is identical to that of the same peak in $[\text{Cr}(\text{tbpy})_3]^{3+}$. We take this as a further experimental validation of the notion that bpy ligands are very weak π -acceptors.⁵⁰ Furthermore, the same peak has been observed at 5990.6 eV for *trans*- $[\text{Cr}^{\text{III}}\text{Cl}_2(\text{OH}_2)_4]\text{Cl}$,⁵¹ which is a *bona fide* Cr^{III} species.

We have also obtained extended X-ray fine structure (EXAFS) data for the $[\text{Cr}(\text{tbpy})_3]^n$ ($n = 3+, 2+, 1+, 0$) series, from which we have obtained average Cr–N bond lengths (Table 6). The data and fits are shown in the Supporting

Table 6. EXAFS Fit Results for the First Coordination Sphere of the $[\text{Cr}(\text{tacn})_2]^{3+/2+}$ and $[\text{Cr}(\text{tbpy})_3]^{3+/2+/1+/0}$

complex	component	R (Å)	σ^2 (Å ²)	ΔE_0 (eV)	error ^a
$[\text{Cr}(\text{tacn})_2]^{3+}$	6 Cr–N	2.08	0.0038	–2.4	0.45
$[\text{Cr}(\text{tacn})_2]^{2+}$	4 Cr–N	2.15	0.0061	–1.6	0.27
	2 Cr–N	2.43	0.0039		
$[\text{Cr}(\text{tbpy})_3]^{3+}$	6 Cr–N	2.04	0.0025	–3.2	0.54
$[\text{Cr}(\text{tbpy})_3]^{2+}$	6 Cr–N	2.03	0.0047	–3.7	0.31
$[\text{Cr}(\text{tbpy})_3]^{1+}$	6 Cr–N	2.01	0.0036	–2.3	0.46
$[\text{Cr}(\text{tbpy})_3]^0$	6 Cr–N	2.00	0.0085	–5.4	0.24

^aError is given by $\Sigma[(\chi_{\text{obsd}} - \chi_{\text{calcd}})^2 k^6] / \Sigma[\chi_{\text{obsd}}^2 k^6]$.

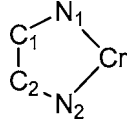
Information. Although the changes are subtle, they are consistent with a *shortening* of the average Cr–N bond upon consecutive one-electron reduction of $[\text{Cr}(\text{tbpy})_3]^{3+}$, in agreement with that observed in the X-ray crystal structures of $[\text{Cr}(\text{tbpy})_3]^n$ ($n = 3+, 2+, 1+$), which we attribute to increased Coulombic attraction of the $(\text{bpy}^*)^{1-}$ radical anion to the Cr^{III} center. In the absence of a crystal structure of $[\text{Cr}(\text{tbpy})_3]^0$, these EXAFS data are used as evidence for an electronic structure description of this species as $[\text{Cr}^{\text{III}}(\text{tbpy}^*)_3]^0$ since it

displays the shortest average Cr–N distance of the series at 2.00(2) Å.

3.6. Broken-Symmetry Density Functional Theory (DFT) Results. When the spin-states of these compounds, the localized quinoidal distortions observed in the X-ray crystal structures of $[\text{Cr}(\text{tbpy})_3]^{2+}$ and $[\text{Cr}(\text{tbpy})_3]^{1+}$, and the XAS and EXAFS data are all taken together, a picture emerges wherein consecutive one-electron reduction of $[\text{Cr}(\text{tbpy})_3]^{3+}$ occurs into localized ligand-centered orbitals which are antiferromagnetically coupled to the high-spin Cr^{III} center. This bonding description requires a small energy gap between a bpy-centered LUMO and the chromium SOMOs. To probe this possibility, we have undertaken a broken-symmetry density functional theory (DFT) study into the electronic structure of these compounds. We assessed the accuracy of our computational results by comparing intraligand bond lengths of the crystalline and geometry-optimized structures as well as the experimental and calculated X-ray absorption spectra. Good agreement between theory and experiment is obtained using the broken-symmetry formalism³⁴ to approximate the true multiconfigurational electronic structures of these species. As such species are not correctly described by a single-determinant wave function, complete active space (CAS) calculations are generally desired for a precise assignment of electronic structure. Unfortunately, these ab initio calculations become prohibitively time- and resource-consuming with increasing molecule size. A convenient single-determinant approximation for the calculation of diradicals was developed by Noodleman³⁴ for calculating antiferromagnetically coupled (i.e., weakly bonded) di- and polynuclear clusters (i.e., metal–metal diradicals). This broken symmetry DFT approach has been successfully applied by a number of groups (e.g., refs 51 and 52) to describe metal–ligand and ligand–ligand diradicals.^{40,41} With the advent of time-dependent DFT (TD-DFT) for the calculation of absorption spectra (i.e., electronic, X-ray), the validity of (broken symmetry) DFT calculations may be scrutinized by comparing the calculated and experimental spectra. Corroboration of experimental (spectroscopic and geometric) and calculated parameters is required to assess the validity of the calculations and the descriptions of the electronic structures derived from them.

In the following, a picture of the electronic structures of complexes $[\text{Cr}(\text{bpy})_3]^n$ ($n = 3+, 2+, 1+, 0, 1-, 2-, 3-$) and $[\text{Cr}(\text{tacn})_2]^{3+/2+}$, as well as $[\text{Cr}(\text{CN})_6]^{3-/4-}$ is derived from (broken symmetry (BS)) DFT calculations by using the B3LYP functional for geometry optimizations, the MO descriptions, and spin distributions in these complexes (Mulliken spin density population analyses). In general, the calculated geometries and experimental metrical parameters of complexes are found to be in reasonable agreement (Table 7). A characteristic feature of the B3LYP functional is the slight overestimation by up to $\sim +0.06$ Å of the calculated metal–ligand bond distances (Cr–C or Cr–N).

3.6.1. Calculated Geometries and Electronic Structures of Complexes 5–8. Given that the octahedral complexes $[\text{Cr}(\text{CN})_6]^{3-/4-}$ possess an $S = 3/2$ and an $S = 1$ ground state, respectively, their ground state geometries were calculated as spin-unrestricted systems (UKS). Their calculated electronic structures are in agreement with their descriptions as a Cr^{III} (d^3) species with three metal-centered SOMOs (Cr character 89.1%) for the trianion **8** ($(t_{2g})^3$) and as low-spin Cr^{II} (d^4) species with a $(t_{2g})^4$ configuration for the tetraanion **7**. Accordingly, the Mulliken spin population analysis shows 3.3

Table 7. Calculated ($[\text{Cr}(\text{bpy})_3]^n$) and Experimental ($[\text{Cr}(\text{bpy})_3]^n$) Bond Lengths (Å)


		$n = 3$		$n = 2$		$n = 1$		$n = 0$
		calcd	exp	calcd	exp	calcd	exp	calcd
bpy ₁	Cr–N ₁	2.094	2.0257(11)	2.111	2.0613(14)	2.064	2.0365(15)	2.065
	Cr–N ₂	2.095	2.0257(11)	2.091	2.0693(14)	2.066	2.0365(15)	2.065
	N ₁ –C ₁	1.364	1.3595(15)	1.361	1.361(2)	1.376	1.362(2)	1.390
	N ₂ –C ₂	1.364	1.3595(15)	1.365	1.357(2)	1.375	1.362(2)	1.390
	C ₁ –C ₂	1.480	1.479(2)	1.477	1.473(2)	1.452	1.460(3)	1.430
bpy ₂	Cr–N ₁	2.094	2.0413(11)	2.112	2.0671(14)	2.065	2.0122(16)	2.064
	Cr–N ₂	2.095	2.0476(11)	2.092	2.0588(14)	2.064	1.9972(15)	2.064
	N ₁ –C ₁	1.364	1.3543(16)	1.361	1.359(2)	1.376	1.373(2)	1.390
	N ₂ –C ₂	1.364	1.3566(16)	1.365	1.358(2)	1.376	1.375(2)	1.390
	C ₁ –C ₂	1.480	1.4787(16)	1.478	1.475(2)	1.452	1.437(2)	1.431
bpy ₃	Cr–N ₁	2.095	2.0413(11)	2.062	1.9942(14)	2.065	2.0122(16)	2.064
	Cr–N ₂	2.095	2.0476(11)	2.062	1.9884(14)	2.065	1.9972(15)	2.064
	N ₁ –C ₁	1.364	1.3543(16)	1.369	1.373(2)	1.375	1.373(2)	1.390
	N ₂ –C ₂	1.364	1.3566(16)	1.369	1.372(2)	1.375	1.375(2)	1.390
	C ₁ –C ₂	1.480	1.4787(16)	1.463	1.452(2)	1.452	1.437(2)	1.431

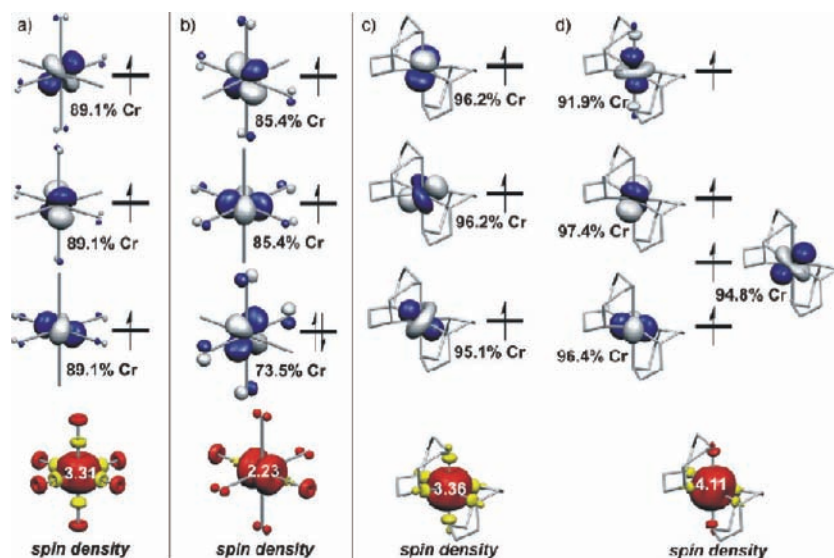


Figure 9. Occupied chromium d-orbitals and spin density distributions (Mulliken) from DFT calculations of (a) $[\text{Cr}^{\text{III}}(\text{CN})_6]^{3-}$ (8), (b) $[\text{Cr}^{\text{II}}(\text{CN})_6]^{4-}$ (7), (c) $[\text{Cr}^{\text{III}}(\text{tacn})_2]^{3+}$ (5), and (d) $[\text{Cr}^{\text{II}}(\text{tacn})_2]^{2+}$ (6).

electrons at the Cr center in the former and 2.2 in the latter (see Figure 9), in agreement with its $S = 1$ ground state.

The structures of complexes $[\text{Cr}(\text{tacn})_2]^{3+/2+}$ with an $S = 3/2$ and $S = 2$ ground state, respectively, have been calculated previously.⁵³ Our results on the geometry optimization agree perfectly with those calculations. Noteworthy is the fact that there are six equivalent Cr–N bonds in the former but two long axial and four shorter equatorial Cr–N bonds (elongated octahedral) in the latter as a consequence of the presence of a central high-spin Cr^{II} ($(t_{2g})^3(e_g)^1$) Jahn–Teller ion. The Mulliken spin density population analysis shows three metal-centered SOMOs (3.4 electrons) for the trication, but four metal-centered SOMOs for the dication (4.1 electrons) (Figure 9).

The above four compounds serve as benchmark species for the Cr K-edge XAS measurements since $[\text{Cr}^{\text{III}}(\text{CN})_6]^{3-}$ and $[\text{Cr}^{\text{III}}(\text{tacn})_2]^{3+}$ both contain a central Cr^{III} ion but the ligands are strong σ -donors and π -acceptors in the former but pure σ -donors in the latter. Similarly, $[\text{Cr}^{\text{II}}(\text{CN})_6]^{4-}$ ($S = 1$) and $[\text{Cr}^{\text{II}}(\text{tacn})_2]^{2+}$ ($S = 2$) allow us to study the effect of a low-spin vs a high-spin d^4 configuration at the central metal ion on the Cr K-pre-edge energies.

3.6.2. Calculated Geometries and Electronic Structures of the Electron Transfer Series $[\text{Cr}(\text{bpy})_3]^n$ ($n = 3+, 2+, 1+, 0$). Table 7 summarizes the experimental (where available) and the geometry-optimized structural data of the respective three bpy ligands and the corresponding Cr–N bond distances in the series. Figure 10 shows MO diagrams of their electronic structures and Mulliken spin density distribution plots.

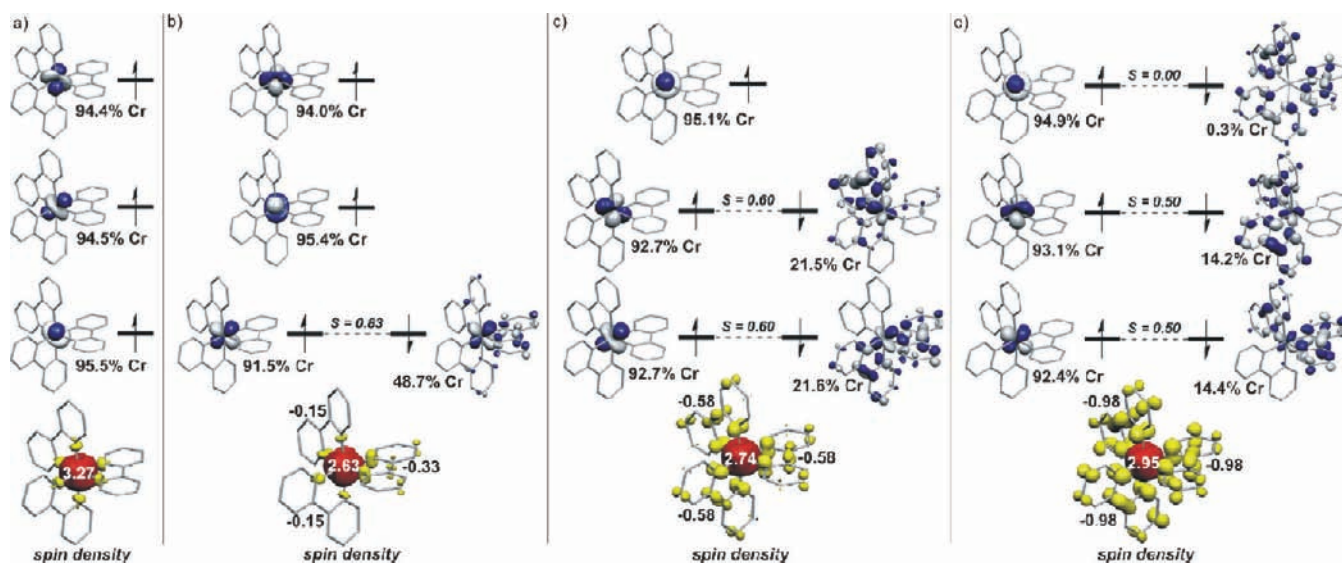


Figure 10. Frontier orbitals and spin density plots from DFT calculations of (a) $[\text{Cr}^{\text{III}}(\text{bpy}^0)_3]^{3+}$, (b) $[\text{Cr}^{\text{III}}(\text{bpy}^0)_2(\text{bpy}^\bullet)]^{2+}$, (c) $[\text{Cr}^{\text{III}}(\text{bpy}^0)(\text{bpy}^\bullet)_2]^+$, and (d) $[\text{Cr}^{\text{III}}(\text{bpy}^\bullet)_3]^0$.

As expected, the trication $[\text{Cr}(\text{bpy})_3]^{3+}$ is a genuine Cr^{III} complex with three metal-centered SOMOs ($\sim 95\%$ Cr) typical for a $(t_{2g})^3$ configuration in an octahedral ligand field. The three N,N' -coordinated bipyridine ligands are equivalent and the $C_{\text{py}}-C_{\text{py}}$ distance at 1.480 Å and the C–N bond lengths at 1.364 Å are typical for three neutral (bpy^0) ligands. The calculated average Cr–N bond is at 2.095 Å whereas the experimental value of 2.038 Å is 0.057 Å shorter, as is expected for the B3LYP functional. The spin density distribution is in agreement with this electronic structure: there are 3.3 electrons at the Cr ion and no significant spin density on the (bpy^0) ligands.

The calculations of the dication $[\text{Cr}(\text{bpy})_3]^{2+}$ ($S = 1$) both as a spin-unrestricted Kohn–Sham (UKS) and as a broken symmetry BS(3,1) calculation converged to the same optimized geometry and electronic structure. The three bpy ligands are *not* fully equivalent: there are two neutral (bpy^0) and one monoanionic $(\text{bpy}^\bullet)^{1-}$ present according to the observed four long Cr–N distances and two shorter ones, respectively. Two $C_{\text{py}}-C_{\text{py}}$ bonds are calculated at 1.477 Å and one slightly shorter bond at 1.463 Å, which agrees well with experiment and indicates significant $(\text{bpy}^\bullet)^{1-}$ character of one of the three bpy ligands. The calculated C1–N1 bond at 1.372 Å is also longer for this $(\text{bpy}^\bullet)^{1-}$ than the same bonds in the two (bpy^0) ligands, at 1.358 Å.

The qualitative MO diagram in Figure 10b identifies three metal-centered SOMOs ($>90\%$ Cr character) typical for a $(t_{2g})^3$ configuration of a Cr^{III} ion. A fourth SOMO possesses 51.3% bpy and 48.7% Cr character that is strongly antiferromagnetically coupled with one of the Cr-based SOMOs ($S = 0.83$) yielding the observed ($S = 1$) ground state. The Mulliken spin density reveals approximately three unpaired electrons (2.6) on chromium and ~ 0.63 electrons distributed over the three bpy ligands: 0.15 electrons each at two bpy ligands and 0.3 electrons at the third. This computational result may be represented by the two following resonance structures: $[\text{Cr}^{\text{III}}(\text{bpy}^0)_2(\text{bpy}^\bullet)]^{2+} \leftrightarrow [\text{Cr}^{\text{II}}(\text{bpy}^0)_3]^{2+}$. The central chromium ion would appear to be a little more reduced than a genuine octahedral Cr^{III}

species and, conversely, a bit more oxidized than a genuine low-spin Cr^{II} complex.

The calculations for the monocation $[\text{Cr}(\text{bpy})_3]^{1+}$ ($S = 1/2$) were performed in the same manner as described above for the dication. The UKS and BS(3,2) solutions are identical. Interestingly, and in contrast to experiment, the three coordinated bpy ligands are calculated to be equivalent. The calculated $C_{\text{py}}-C_{\text{py}}$ bond length at 1.452 Å and the C–N bonds at 1.376 Å indicate a high degree of reduction to $(\text{bpy}^\bullet)^{1-}$ radicals. The Mulliken spin density population analysis indicates the presence of 1.74 electrons distributed evenly over the three bpy ligands. Three metal-centered SOMOs are indicative of a $(t_{2g})^3$ Cr^{III} configuration and two ligand-based SOMOs are identified with only $\sim 22\%$ Cr character that are strongly antiferromagnetically coupled to two metal-based SOMOs giving rise to the observed $S = 1/2$ ground state, where the unpaired electron resides in a 3d metal orbital. This is in agreement with the reported EPR spectrum of the monocation, which displays large ^{53}Cr hyperfine coupling.⁵⁴ The fact that a delocalized model has been computationally obtained for the monocation is most probably due to the known bias of the B3LYP functional used here.

Calculations for the diamagnetic neutral complex $[\text{Cr}(\text{bpy})_3]^0$ ($S = 0$) have been performed by using the spin-restricted Kohn–Sham (RKS) and a BS(3,3) approach. The former afforded a solution which was 30.6 kcal/mol (!) higher in energy than the latter. Therefore, we consider only the BS(3,3) solution in the following.

Geometry optimization shows that this neutral species contains three equivalent N,N' -coordinated π -radical anions $(\text{bpy}^\bullet)^{1-}$: the average $C_{\text{py}}-C_{\text{py}}$ bonds are short at 1.430 Å as has been experimentally observed for the sodium salt of the radical anion.⁵ Consequently, the central chromium ion possesses an oxidation state of +III with a $(t_{2g})^3$ configuration. These three metal-centered SOMOs are intramolecularly antiferromagnetically coupled to the corresponding three ligand-centered SOMOs affording the observed $S = 0$ ground state. We have also examined the high-spin and BS(3,3) energies together with the corresponding spin-expectation values $\langle S^2 \rangle$ according to the

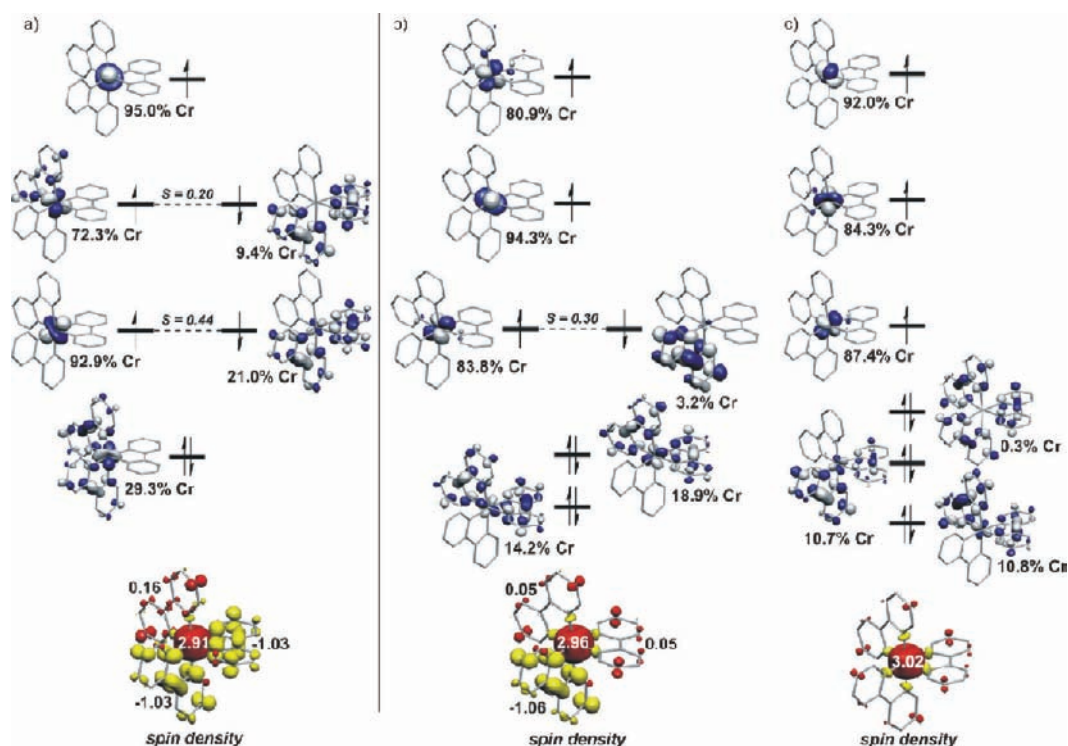


Figure 11. Qualitative MO scheme and calculated Mulliken spin density (below) of (a) $[\text{Cr}^{\text{III}}(\text{bpy}^\bullet)(\text{bpy}^{2-})]^{1-}$ ($S = 1/2$), (b) $[\text{Cr}^{\text{III}}(\text{bpy}^\bullet)(\text{bpy}^{2-})_2]^{2-}$ ($S = 1$), and (c) $[\text{Cr}^{\text{III}}(\text{bpy}^{2-})_3]^{3-}$ ($S = 3/2$).

Yamaguchi approach,⁵⁵ eqs 1 and 2. The meaning of $\langle S^2 \rangle$ has been described in ref 55.

$$J = \frac{E_{\text{HS}} - E_{\text{BS}}}{\langle S^2 \rangle_{\text{HS}} - \langle S^2 \rangle_{\text{BS}}} \quad (2)$$

The numerical value of the exchange coupling constant J estimated in this fashion is -599 cm^{-1} in excellent agreement with the experimental value of -477 cm^{-1} .

The spin density plot for $[\text{Cr}(\text{bpy})_3]^0$ shown in Figure 10d exhibits ~ 3 electrons located at the central metal ion Cr^{III} and ~ 1.0 electron on each bpy ligand. Thus, the electronic structure is best described as $[\text{Cr}^{\text{III}}(\text{bpy}^\bullet)_3]^0$.

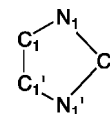
3.6.3. Calculated Geometries and Electronic Structures of the Electron Transfer Series $[\text{Cr}(\text{bpy})_3]^n$ ($n = 1-, 2-, 3-$). Structural and spectroscopic data for the anionic complexes $[\text{Cr}(\text{bpy})_3]^n$ ($n = 1-, 2-, 3-$) have not been reported to date, but from their magnetic susceptibility measurements at room temperature their electronic ground states have been established (see Table 2): the monoanion possesses an $S = 1/2$, the dianion an $S = 1$, and the trianion an $S = 3/2$ ground state. Despite this dearth of experimental (spectroscopic and structural) data on the anions, we present here our computational results, which were obtained in the same manner as described above for the cationic and neutral species. Figure 11 displays qualitative MO diagrams and spin density plots and Table 8 summarizes the calculated metrical details of the three bpy ligands in each of the three anionic species.

Geometry optimizations for the mono- and dianion were carried out by employing both the UKS and BS(3,2)/BS(3,1) method, respectively, whereas for the trianion only the UKS calculations were carried out. Interestingly, both approaches for the mono- and dianion converged to the same broken symmetry solution.

The geometry of the bpy ligands in the monoanion displays the characteristic features of a single, diamagnetic $(\text{bpy}^{2-})^{2-}$ dianion and two π -radical monoanions $(\text{bpy}^\bullet)^{1-}$. The respective $\text{C}_{\text{py}}-\text{C}_{\text{py}}$ and $\text{C}-\text{N}$ bond distances agree nicely with those summarized in Table 1 for the alkali salts of $(\text{bpy}^\bullet)^{1-}$ and $(\text{bpy}^{2-})^{2-}$. The optimized geometry of the dianion $[\text{Cr}(\text{bpy})_3]^{2-}$ displays the same features but now *two* $(\text{bpy}^{2-})^{2-}$ dianions and a *single* $(\text{bpy}^\bullet)^{1-}$ π -radical monoanion are present. In both cases the oxidation levels of the N, N' -coordinated bpy ligands are calculated to be *localized*.

Table 8. Calculated Bond Lengths (Å) for $[(\text{bpy})_3\text{Cr}]^n$ ($n = 1-, 2-, 3-$) using COSMO³³

		$n = 1-$	$n = 2-$	$n = 3-$
bpy ₁	Cr–N ₁	2.077	2.101	2.076
	Cr–N ₁ '	2.092	2.100	2.075
	N ₁ –C ₁	1.391	1.392	1.434
	N ₁ '–C ₁ '	1.392	1.392	1.434
	C ₁ –C ₁ '	1.430	1.429	1.388
bpy ₂	Cr–N ₁	2.077	2.063	2.076
	Cr–N ₁ '	2.091	2.048	2.075
	N ₁ –C ₁	1.391	1.432	1.434
	N ₁ '–C ₁ '	1.392	1.432	1.434
	C ₁ –C ₁ '	1.430	1.390	1.388
bpy ₃	Cr–N ₁	2.038	2.063	2.076
	Cr–N ₁ '	2.037	2.048	2.076
	N ₁ –C ₁	1.428	1.432	1.435
	N ₁ '–C ₁ '	1.428	1.432	1.434
	C ₁ –C ₁ '	1.393	1.390	1.388



The optimized geometry of the trianion $[\text{Cr}(\text{bpy})_3]^{3-}$ exhibits the presence of three equivalent N,N' -coordinated dianionic $(\text{bpy}^{2-})^{2-}$ ligands. Very similar experimental structures have been reported for $[\text{Zr}^{\text{IV}}(\text{bpy}^{2-})_3]^{2-56}$ and $[\text{Al}^{\text{III}}(\text{bpy}^{2-})_2]^{1-57}$.

The above oxidation level distribution in all three complexes renders the oxidation state of the central Cr ion invariably +III (d^3). The calculated electronic structures and spin densities at the central Cr ion of 2.91 electrons in the monoanion, 2.96 in the dianion, and 3.02 in the trianion nicely corroborate this notion. Similarly, the two $(\text{bpy}^\bullet)^{1-}$ ligands in the monoanion carry each one unpaired electron as does the single π -radical anion $(\text{bpy}^\bullet)^{1-}$ in the dianionic species.

The spins of the ligand-centered π -radicals in the mono- and dianions couple strongly in an antiferromagnetic fashion to the $S_{\text{Cr}} = 3/2$ local spin state ($J = -365$ and -82 cm^{-1} , respectively) yielding the observed double and triplet ground state for $[\text{Cr}^{\text{III}}(\text{bpy}^\bullet)_2(\text{bpy}^{2-})]^{1-}$ and $[\text{Cr}^{\text{III}}(\text{bpy}^\bullet)(\text{bpy}^{2-})_2]^{2-}$, respectively. The trianion represents then a classic octahedral Werner complex of Cr^{III} with a metal-centered $(t_{2g})^3$ configuration and three closed-shell bidentate $(\text{bpy}^{2-})^{2-}$ ligands.

3.6.4. Calculated Cr K-Pre-edge Spectra of Complexes. Recently, a simple time-dependent DFT (TD-DFT) approach was developed for the calculation of pre-edge XAS spectra^{35,36} and successfully utilized in assigning S, Cl, Mn, Fe, and Cr K-edge spectra.^{38,58,59} We have used this method here for calculating the Cr K-edge spectra of complexes 1–8. The pre-edge region of the Cr K-edge spectra reveal peaks from weak quadrupole-allowed $1s$ to $3d$ transitions, which primarily gain intensity through mixing of $4p$ character into these orbitals giving the transitions significant electric dipole character. The experimental and calculated Cr K-pre-edge spectra are shown in Figure 12 and 13 and Table 5 and show very good agreement

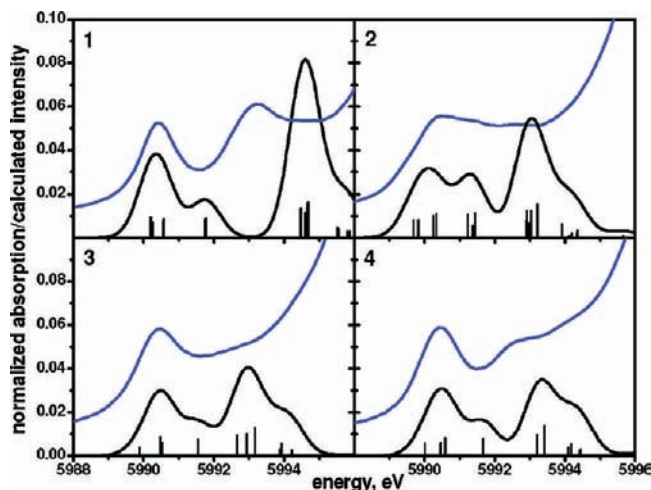


Figure 12. Experimental (blue) vs calculated (black) chromium K-pre-edge X-ray absorption spectra of $[(\text{bpy})_n\text{Cr}]^n$ ($n = 3+$ (1), $2+$ (2), $1+$ (3), 0 (4)). Calculated spectra modeled with 1.0 eV line broadening. Individual transitions are shown as black columns.

for the position of the first transition after applying an empirical +125.79 eV correction to the calculated values. Here again, we rely on the position of the first pre-edge transition to assess the agreement between our experimental and calculated values. We note that the higher-energy transitions do not show good agreement, consistent with these transitions having significant

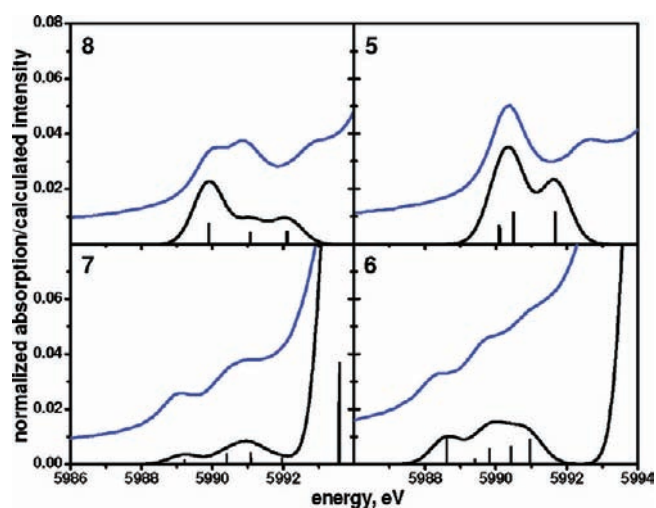


Figure 13. Experimental (blue) vs calculated (black) chromium K-pre-edge X-ray absorption spectra of $[(\text{CN})_6\text{Cr}]^{3-}$ (8), $[(\text{CN})_6\text{Cr}]^{4+}$ (7), $[(\text{tacn})_2\text{Cr}]^{3+}$ (5), and $[(\text{tacn})_2\text{Cr}]^{2+}$ (6).

metal-to-ligand charge transfer ($1s$ to $\text{bpy} \pi^*$) character that TD-DFT does not effectively model.⁶⁰

The stick plots in Figures 12–14 show the sum of the dipole and quadrupole contributions to the calculated transition intensities and the composition of the acceptor MOs are listed in Table S5. Despite the low Cr $3d$ content of these MOs, they are relatively intense because of a small but crucial contribution from the Cr $4p$ orbitals. The first peak in all spectra comprises the $1s$ to $t_{2g}(\beta)$ and $1s$ to $e_g(\alpha)$ transitions (labeled 1 and 2 in the stick spectrum of Figure 14). For Cr^{III} species 1–4 and 5 this peak is observed and calculated at 5990.4 ± 0.2 eV in very good agreement with the peak at 5990.6 eV observed for $\text{trans}[\text{Cr}^{\text{III}}\text{Cl}_2(\text{OH}_2)_4]\text{Cl}$.

The two transitions comprising the second peak at 5991.7 eV in Figure 14 (labeled 3 in the stick spectrum) are the $1s$ excitation to the $e_g(\beta)$ orbitals. The third intense peak at 5994.6 eV (labeled 4 + 5 in the stick spectrum) comprises the transitions $1s$ to $\pi^*(\text{bpy}^0)$. The third peak is absent in the spectra of 5 and 6.

It is important to note that the calculated energies of the first peaks of the pairs 5 and 6 differ by 1.7 eV and for 8 and 7 by 1.1 eV, indicating a change of oxidation state by one unit from +III to +II irrespective of the spin state of the Cr(II) species (high-spin in 6 but low-spin in 7). The calculations nicely corroborate the experimental findings.

4. DISCUSSION

The stepwise one-electron reduction of neutral 2,2'-bipyridine via the π -radical monoanion and finally to the diamagnetic dianion is formally a stepwise dearomatization of the two C–C coupled aromatic pyridine rings in (bpy^0) . In a molecular orbital description, the energetically high-lying LUMO of neutral (bpy^0) is filled first with one electron in $(\text{bpy}^\bullet)^{1-}$ (now a SOMO) and then with a second electron in $(\text{bpy}^{2-})^{2-}$ (now a HOMO). These steps are accompanied by significant structural changes of which the change for the $C_{\text{py}}-C_{\text{py}}$ bond is the most dramatic ($\sim 1.47 \pm 0.01$ Å in (bpy^0) , 1.43 ± 0.01 Å in $(\text{bpy}^\bullet)^{1-}$, and 1.38 ± 0.01 Å in $(\text{bpy}^{2-})^{2-}$). The C–N distances of the α -diimine chelate ring $M(\text{bpy})$ are also indicative of these reductions: the C–N bonds are short at 1.35 ± 0.01 Å in (bpy^0) , longer at 1.39 ± 0.01 Å in $(\text{bpy}^\bullet)^{1-}$, and even longer at

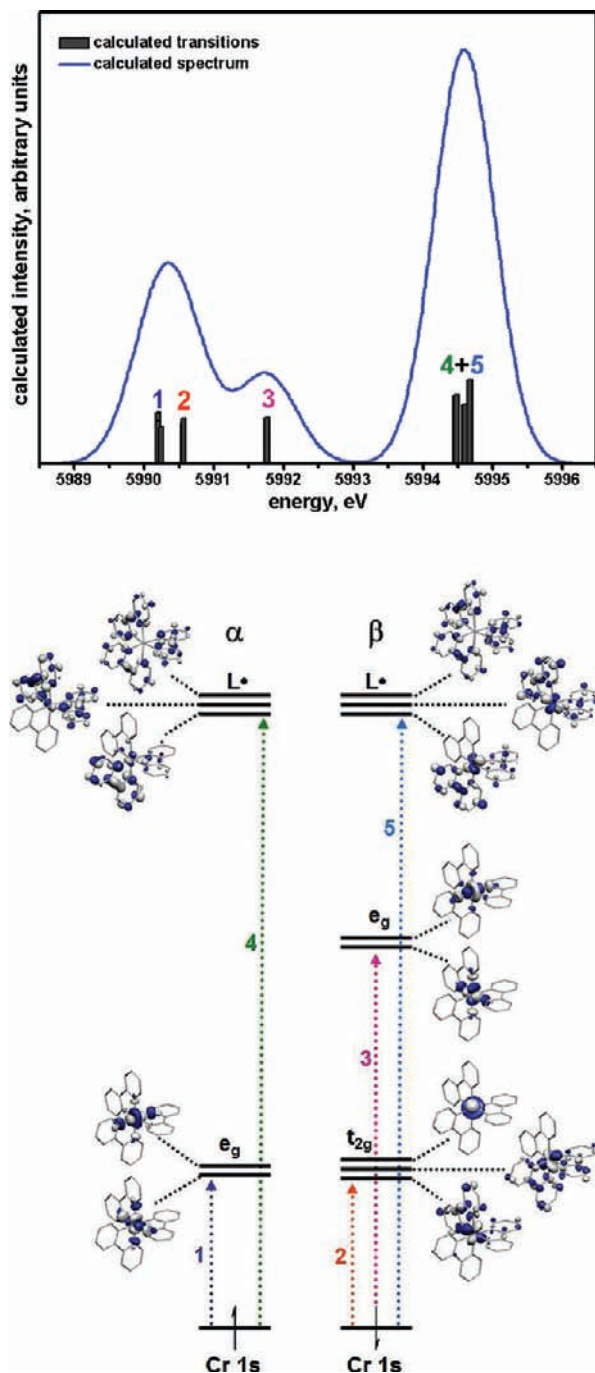


Figure 14. Top: Simulated Cr K-pre-edge spectrum of $[\text{Cr}^{\text{III}}(\text{bpy}^0)_3]^{3+}$ (blue line) and stick plot individual transitions. The total calculated intensity represents the sum of the dipole and quadrupole contributions. Bottom: A qualitative MO scheme presenting the lowest unoccupied orbitals derived from a B3LYP DFT calculation and the four transitions that comprise the calculated pre-edge. The MO compositions are displayed in S5.

$1.44 \pm 0.01 \text{ \AA}$ in $(\text{bpy}^{2-})^{2-}$ (see Table 1). For instance, in neutral $[(\text{CO})_4\text{Cr}(\text{bpy})]^0$, the $\text{C}_{\text{py}}-\text{C}_{\text{py}}$ distance of the N,N' -coordinated (bpy^0) is determined crystallographically at $1.471(5) \text{ \AA}$ and the C–N distance is found at $1.348(4) \text{ \AA}$.⁶¹ Cr^0 with a d^6 low-spin configuration is, in principle, a strong π -donor but the N,N' -coordinated (bpy^0) is a weak π -acceptor.⁵⁰ Therefore, we do not observe metal-to-ligand π -backdonation effects which would lead to structural changes in the (bpy^0)

ligand (making it more reduced). This is a consequence of the fact that the energy difference between the LUMO of the (bpy^0) ligand and the (t_{2g}) orbitals of the d^6 configuration at the metal center is quite large. In the monoanion $[(\text{CO})_4\text{Cr}^0(\text{bpy}^*)]^{1-}$ ($S = 1/2$),⁶² the unpaired electron resides >95% in the bpy ligand as DFT calculations and EPR spectroscopy have demonstrated.⁶³ Here, the $\text{C}_{\text{py}}-\text{C}_{\text{py}}$ and C–N distances have been calculated⁶⁴ by us to be 1.423 \AA and 1.392 \AA , respectively, in excellent agreement with the sodium salt of $(\text{bpy}^*)^{1-}$.⁶ As pointed out by Vlček et al.,⁶³ “on reduction, the $[(\text{bpy}^0)]$ ligand changes from a weak π -acceptor to a π -donor.” This is strong evidence that there are no structural changes to be expected in the (bpy^0) ligand when a “low-valent” transition metal ion is N,N' -coordinated to a neutral (bpy^0) ligand. This has been incorrectly invoked for a number of organometallic coordination complexes containing coordinated bpy ligands with unusual structural distortions (always shorter $\text{C}_{\text{py}}-\text{C}_{\text{py}}$ and longer C–N bonds).⁶⁷

In the monocation $[(\text{CO})_4\text{Cr}^{\text{I}}(\text{bpy}^0)]^{1+}$ ($S = 1/2$), the DFT calculations clearly show that the one-electron oxidation is metal-centered,⁶⁵ generating a low-spin Cr^{I} species (d^5 , $S = 1/2$) with a neutral (bpy^0) ligand ($\text{C}_{\text{py}}-\text{C}_{\text{py}}$ at 1.477 \AA and C–N at 1.359 \AA). For the present series of complexes, this implies that, since Cr^{III} and Cr^{II} are very weak π -donors and (bpy^0) is a very weak π -acceptor, the $\text{C}_{\text{py}}-\text{C}_{\text{py}}$ and C–N bonds in five-membered $\text{Cr}^{\text{III}}(\text{bpy}^0)$ rings are virtually identical to those of the uncoordinated (bpy^0) ligand. Furthermore, N,N' -coordinated $\text{Cr}^{\text{III}}(\text{bpy}^*)$ rings are also expected to show $\text{C}_{\text{py}}-\text{C}_{\text{py}}$ and C–N bond distances nearly identical to those in the sodium or potassium salts of $(\text{bpy}^*)^{1-}$. It is only the $\text{Cr}^{\text{III}}(\text{bpy}^{2-})$ unit which is expected to display significant ligand-to-metal π -donation, which may result in some elongation of the $\text{C}_{\text{py}}-\text{C}_{\text{py}}$ bond and concomitant shortening of the C–N distances that may resemble the geometric details as in $\text{Cr}(\text{bpy}^*)$.⁶⁷

In tris(bpy) metal complexes containing three N,N' -coordinated bpy ligands in two different oxidation levels, it is not possible to distinguish between an N,N' -coordinated (bpy^0) , a π -radical anion $(\text{bpy}^*)^{1-}$, and a dianion $(\text{bpy}^{2-})^{2-}$ by single-crystal X-ray crystallography if the tris(bpy)M moiety possesses crystallographically imposed C_3 site symmetry. This has been shown to be the case for $[\text{Cr}(\text{bpy})_3](\text{PF}_6)_n$ ($n = 3+, 2+, 1+$) series. On the other hand, if this moiety possesses only C_2 site symmetry as in the present cases 1 and 3, it is possible to distinguish between the above oxidation levels provided that no static disorder problems prevail.

The average Cr–N distances in complexes 1–3 measured by single-crystal X-ray crystallography disclose an interesting experimental trend: this average Cr–N distance decreases with decreasing charge of the respective complex ranging from $3+$ in 1 to $1+$ in 3 (Table 7). This trend is nicely reproduced by the DFT calculations using the B3LYP functional, although the absolute values are calculated to be $\sim 0.06 \text{ \AA}$ longer than the values determined by EXAFS. We interpret this behavior as a manifestation of a purely electrostatic effect, where the neutral N,N' -coordinated (bpy^0) ligand has two longer Cr–N bonds than the corresponding distances of a $(\text{bpy}^*)^{1-}$ π -radical anion both interacting with a Cr^{III} cation. In going stepwise from 1 with three neutral (bpy^0) to 4 with three $(\text{bpy}^*)^{1-}$ ligands, a nearly linear shrinking of the average Cr–N distance is calculated and observed (for complexes 1–3). This trend is reversed on going from the neutral species 4 to the mono-, di-, and trianion because we accumulate negatively charged mono- and dianions, $(\text{bpy}^*)^{1-}$ and $(\text{bpy}^{2-})^{2-}$, around the central Cr^{III} cation,

which effectively results in electrostatic repulsion of the ligands with concomitant increases of the average Cr–N bond as revealed by our calculations (Table 8). Thus, the structural investigation of complexes 1–3 and the calculated values for $[\text{Cr}(\text{bpy})_3]^{0,1-,2-,3-}$ suggest that the complete redox series involves ligand-based one-electron redox reactions and that the central chromium ion possesses, invariably, a +III oxidation level (d^3 configuration). No significant metal-to-ligand π -backdonation or ligand-to-metal π -donation effects have been identified.

The X-ray absorption spectra provide the most compelling evidence that complexes 1–4 of the electron transfer series all contain a central Cr^{III} ion. The energy of the corresponding first Cr K-pre-edge peak is invariably observed at 5990.4 eV in agreement with that of *trans*- $[\text{Cr}^{\text{III}}\text{Cl}_2(\text{OH}_2)_4]\text{Cl}^{51}$ and 5. This peak corresponds to 1s to 3d transitions and is a very sensitive marker for the oxidation state of the central chromium ion in an octahedral complex. Interestingly, the same pre-edge peaks at very similar energies are observed for complexes with six oxygen donor atoms as in $[\text{Cr}^{\text{III}}(3,6\text{L}_{\text{sq}}^{\bullet})_3]^{0}$ ($S = 0$) (5990.7 eV) or $[\text{Cr}^{\text{III}}(3,6\text{L}_{\text{sq}}^{\bullet})_2(3,6\text{L}_{\text{cat}})]^{1-}$ ($S = 1/2$) (5990.7 eV), and six sulfur atoms as in $[\text{Cr}^{\text{III}}(\text{mnt})_3]^{3-}$ ($S = 3/2$) (5990.3 eV), where $(3,6\text{L}_{\text{sq}}^{\bullet})$ represents 3,6-di-*tert*-butylbenzosemiquinonate (1 $-$) and $(3,6\text{L}_{\text{cat}})$ is its one-electron reduced dianion; $(\text{mnt})^{2-}$ is maleonitrile dithiolate (2 $-$).⁵¹ In all cases, the N, O, and S donor ligands are strong σ -donor ligands and the O, S ligands are reasonably strong π -donor ligands. When π -acceptors such as cyanide, as in $[\text{Cr}^{\text{III}}(\text{CN})_6]^{3-}$, are present, the Cr K-pre-edge peak is shifted to lower energies by only ~ 0.2 eV. A full one-electron reduction of the central Cr^{III} ion shifts the Cr K-pre-edge energy by 1.1 eV (8 to 7) or 1.7 eV (5 to 6) to lower energies, depending on the spin state of the resulting Cr^{II} ion (low-spin or high-spin Cr^{II} , respectively). These experimental observations are in excellent agreement with the electronic structure calculations.

Thus, these experiments unequivocally establish that the $[\text{Cr}(\text{bpy})_3]^{2+}$ species cannot possess an electronic structure $[\text{Cr}^{\text{II}}(\text{bpy}^0)_3]^{2+}$ ($S = 1$) comprised of three neutral (bpy^0) ligands and a central low-spin Cr^{II} ion.¹¹ As we will show in a forthcoming paper, the same holds true for $[\text{Cr}(\text{phen})_3]^{2+}$ and $[\text{Cr}(\text{terpy})_2]^{2+}$, where phen represents 1,10-phenanthroline and terpy is 2,2':6',2''-terpyridine.

The electronic structure of the neutral diamagnetic complex 4 has, in the past, often been discussed but controversially with respect to questions like (a) how much electron density resides in the π^* -LUMO of the (bpy^0) ligands, (b) if one or more of the bpy ligands are reduced, is it localized or delocalized, and (c) can one assign an oxidation state to the central Cr ion or not? The molecular structure of $[\text{Cr}(\text{bpy})_3]^{0}$ has not been solved by X-ray crystallography^{8,9} due to the fact that it crystallizes as a merohedric twin (space group $P\bar{3}c1$). We have also not been able to solve the crystal structure of 4. On the other hand, a number of neutral, diamagnetic tris(benzosemiquinonato)chromium(III) complexes have been structurally characterized.⁶⁶ All of these display a nearly perfect octahedral $\text{Cr}^{\text{III}}\text{O}_6$ polyhedron and their Cr K-pre-edge energy at 5990.7 eV⁵¹ indicative of a central Cr^{III} ion matches the data for 4 very well. The DFT calculations also support the notion of an electronic structure as in $[\text{Cr}^{\text{III}}(\text{bpy}^{\bullet})_3]^{0}$. The electronic spectrum displays intense absorptions in the visible characteristic for N,N' -coordinated (bpy^{\bullet})¹⁻ radical anions.¹⁰ The temperature-dependent magnetic susceptibility of 4 has been successfully modeled by invoking a (strong) intramolecular antiferromagnetic coupling between the spins of the unpaired electrons of the

central Cr^{III} ion ($(t_{2g})^3$) and the three spins of the three (bpy^{\bullet})¹⁻ π -radical anions. Thus, excellent agreement between theory and experiment has been achieved for the electronic (and, to a lesser degree, the molecular) structure of neutral 4. These results emphasize the strength of the DFT calculations.

The molecular and electronic structures of the three anions $[\text{Cr}(\text{bpy})_3]^{1-,2-,3-}$ have been calculated by DFT methodology. The results allow us to propose the following molecular and electronic structures:

- (1) In all three species, the central chromium ion possesses a +III oxidation state ($(t_{2g})^3$ configuration).
- (2) The three one-electron reductions are ligand-based, where the three N,N' -coordinated (bpy^{\bullet})¹⁻ radical monoanions in neutral $[\text{Cr}^{\text{III}}(\text{bpy}^{\bullet})_3]^{0}$ are stepwise reduced to ultimately three N,N' -coordinated (bpy^{2-})²⁻ dianions in $[\text{Cr}^{\text{III}}(\text{bpy}^{2-})_3]^{3-}$.
- (3) The respective ground state of $S = 1/2$ in the monoanion $[\text{Cr}^{\text{III}}(\text{bpy}^{\bullet})_2(\text{bpy}^{2-})]^{1-}$, of $S = 1$ in the corresponding dianion $[\text{Cr}^{\text{III}}(\text{bpy}^{\bullet})(\text{bpy}^{2-})_2]^{2-}$ and of $S = 3/2$ in the trianion $[\text{Cr}^{\text{III}}(\text{bpy}^{2-})_3]^{3-}$ is achieved via strong intramolecular antiferromagnetic coupling between two, one, and no (bpy^{\bullet})¹⁻ radical anionic ligands and a central Cr^{III} ion.
- (4) In the gas phase, the (bpy^{\bullet})¹⁻ and (bpy^{2-})²⁻ ligands are localized and geometrical features of the (bpy^{2-})²⁻ ligands closely resemble those reported for $[\text{Al}^{\text{III}}(\text{bpy}^{2-})_2]^{1-}$ ⁵⁷ and $[\text{Zr}^{\text{IV}}(\text{bpy}^{2-})_3]^{2-}$.⁵⁶

It is unfortunate that, at this point in time, we cannot validate these calculations due to the dearth of available experimental data of these anionic species.

CONCLUSION

We have unambiguously shown by a combination of experimental data (X-ray absorption spectroscopy, single-crystal X-ray absorption spectroscopy, electronic absorption spectroscopy, magnetochemistry, electrochemistry, electron spin resonance spectroscopy) and density functional theoretical calculations that the seven-membered electron transfer series $[\text{Cr}(\text{bpy})_3]^n$ ($n = 3+, 2+, 1+, 0, 1-, 2-, 3-$) involves stepwise one-electron ligand-based reductions: $(\text{bpy}^0) \xrightarrow{e^-} (\text{bpy}^{\bullet})^{1-} \xrightarrow{e^-} (\text{bpy}^{2-})^{2-}$. In species with ligand mixed valency containing $(\text{bpy}^0)/(\text{bpy}^{\bullet})^{1-}$ as in the di- and monocationic species or $(\text{bpy}^{\bullet})^{1-}/(\text{bpy}^{2-})^{2-}$ as in the mono- and dianionic species, these ligand types are localized. All seven members contain a central Cr^{III} ion. The electronic structure of the dication cannot be described as a “low-spin Cr^{II} ” species.

ASSOCIATED CONTENT

Supporting Information

X-ray crystallographic data files (CIF) of compounds 1–3 and 5–6, X-band EPR spectrum of 3, electronic absorption spectrum of 6, X-ray crystallographic data collection and refinement of the structures, IR spectra of complexes 1–4, temperature-dependent magnetic susceptibility data for complexes 1–8, EXAFS data for complexes 1–6, geometry-optimized molecular xyz coordinates for complexes 1–8, effect of COSMO on calculated electronic structures and X-ray absorption spectra, absolute energies, atomic charge and spin density distributions, and calculated Cr 3d and 4p character of orbitals excited into from the Cr 1s orbital in the calculated XAS spectra of complexes 1–8 from TD-DFT. This material is available free of charge via the Internet at <http://pubs.acs.org>.

AUTHOR INFORMATION

Corresponding Author

*E-mail: wieghardt@mpi-muelheim.mpg.de.

Present Addresses

[‡]Department of Chemistry, Emory University, Atlanta, GA 30322, U.S.A.

[§]EPSRC National UK EPR Facility and Service, Photon Science Institute, The University of Manchester, Oxford Road, U.K.

ACKNOWLEDGMENTS

C.S. is grateful to the Alexander von Humboldt foundation for a postdoctoral research fellowship. We thank Heike Schucht and Andreas Göbels for technical assistance. S.D. thanks Cornell University for startup funds. Portions of this research were carried out at the Stanford Synchrotron Radiation Lightsource, a Directorate of SLAC National Accelerator Laboratory and an Office of Science User Facility operated by the U.S. Department of Energy Office of Science by Stanford University. The SSRL Structural Molecular Biology Program is supported by the DOE Office of Biological and Environmental Research, and by the National Institutes of Health, National Center for Research Resources, Biomedical Technology Program.

REFERENCES

- (1) (a) Constable, E. C.; Sykes, A. G. In *Advances in Inorganic Chemistry*; Academic Press: 1989; Vol. 34, p 1. (b) *Comprehensive Coordination Chemistry*; Wilkinson, G., Ed.; Pergamon Press: 1987; Vol. 1–7.
- (2) Throughout this paper, we use the abbreviation (bpy) in a generic sense; no specific oxidation level is implied. When we intend to assign a specific oxidation level to the 2,2'-bipyridines ligand, we use (bpy⁰) for neutral diamagnetic ligand, (bpy[•])¹⁻ for the π -radical monoanion, and (bpy²⁻)²⁻ for the diamagnetic dianion.
- (3) Robin, M. B.; Day, P.; Emel us, H. J.; Sharpe, A. G. In *Advances in Inorganic Chemistry*; Academic Press: 1968; Vol. 10, p 247.
- (4) Chisholm, M. H.; Huffman, J. C.; Rothwell, I. P.; Bradley, P. G.; Kress, N.; Woodruff, W. H. *J. Am. Chem. Soc.* **1981**, *103*, 4945.
- (5) (a) Gore-Randall, E.; Irwin, M.; Denning, M. S.; Goicoechea, J. M. *Inorg. Chem.* **2009**, *48*, 8304. (b) Echegoyen, L.; DeCian, A.; Fischer, J.; Lehn, J.-M. *Angew. Chem., Int. Ed.* **1991**, *30*, 838.
- (6) Bock, H.; Lehn, J.-M.; Pauls, J.; Holl, S.; Krenzel, V. *Angew. Chem., Int. Ed.* **1999**, *38*, 952.
- (7) Crystal structure of [Cr^{III}(bpy⁰)₃](PF₆)₃: (a) Goodwin, K. V.; Pennington, W. T.; Petersen, J. D. *Inorg. Chem.* **1989**, *28*, 2016. (b) Hauser, A.; Maeder, M.; Robinson, W. T.; Murugesan, R.; Ferguson, J. *Inorg. Chem.* **1987**, *26*, 1331.
- (8) Crystal structures of [Cr(bpy)₃](PF₆)₂ and [Cr(bpy)₃](PF₆)₃: Brey, J.; Zwicknagel, A. *Z. Naturforsch., B: Chem. Sci.* **2004**, *59*, 1015.
- (9) For neutral [Cr(bpy)₃]⁰ only the space group has been determined: Albrecht, G. *Z. Chem.* **1963**, *3*, 182. An average Cr–N bond length of 2.08 ± 0.03 Å has been calculated.
- (10) (a) K nig, E.; Herzog, S. *J. Inorg. Nucl. Chem.* **1970**, *32*, 585. (b) Pappalardo, R. *Inorg. Chim. Acta* **1968**, *2*, 209. (c) Kaizu, Y.; Yazaki, T.; Torii, Y.; Kobayashi, H. *Bull. Chem. Soc. Jpn.* **1970**, *43*, 2068. (d) Hanazaki, I.; Nagakura, S. *Bull. Chem. Soc. Jpn.* **1971**, *44*, 2312. (e) Fujita, I.; Yazaki, T.; Torii, Y.; Kobayashi, H. *Bull. Chem. Soc. Jpn.* **1972**, *45*, 2156.
- (11) Textbooks in which the [Cr(bpy)₃]²⁺ ion is described as “low-spin chromium(II)”, that is, [Cr^{II}(bpy⁰)₃]²⁺ (S = 1): (a) Cotton, F. A.; Wilkinson, G.; Murillo, C. A.; Bochmann, M. *Advanced Inorganic Chemistry*, 6th ed.; J. Wiley & Sons: 1999. (b) Greenwood, N. N.; Earnshaw, A. *Chemistry of the Elements*. Wheaton, A. & Co. Ltd.: Exeter, Great Britain, 1988; p 1201. (c) Hollemann, F.; Wiberg, E. *Lehrbuch der Anorganischen Chemie*; deGruyter: Berlin, 1995, p 1455. (d) Larkworthy, L. F.; Nolan, K. B.; O'Brien, P. *Comprehensive Coordination Chemistry*; Wilkinson, G., Gillard, R. D., McCleverty, J. A., Eds.; Pergamon Press: 1987; Vol. 3, p 712. (12) Herzog, S.; Grimm, U.; Waicenbauer, W. *Z. Chem.* **1967**, *7*, 355. (13) Taube, R.; Herzog, S. *Z. Chem.* **1962**, *2*, 225. (14) Wieghardt, K.; Schmidt, W.; Herrmann, W.; Kueppers, H. *J. Inorg. Chem.* **1983**, *22*, 2953. (15) Eaton, J. P.; Nicholls, D. *Trans. Met. Chem.* **1981**, *6*, 203. (16) Scarborough, C. C.; Wieghardt, K. Manuscript in preparation. (17) See also recent examples: (a) Irwin, M.; Jenkins, R. K.; Denning, M. S.; Kr amer, T.; Grandjean, F.; Long, G. J.; Herchel, R.; McGrady, J. E.; Goicoechea, J. M. *Inorg. Chem.* **2010**, *49*, 6160. (b) Kraft, S. J.; Fanwick, P. E.; Bart, S. C. *Inorg. Chem.* **2010**, *49*, 1103. (18) Hein, F.; Herzog, S. *Z. Anorg. Allg. Chem.* **1952**, *267*, 337. (19) (a) Herzog, S.; Renner, K. C.; Sch on, W. *Z. Naturforsch.* **1957**, *12b*, 809. (b) Behrens, H.; M uller, A. *Z. Anorg. Allg. Chem.* **1965**, *341*, 124. (c) Quirk, J.; Wilkinson, G. *Polyhedron* **1982**, *1*, 209. (20) George, G. N. EXAFSPAK; Stanford Synchrotron Radiation Laboratory, Stanford Linear Accelerator Center, Stanford University: Stanford, CA, 2000. (21) Tenderholt, A. PYSpline; Stanford Synchrotron Radiation Laboratory, Stanford Linear Accelerator Center, Stanford University: Stanford, CA, 2005. (22) Mustre de Leon, J.; Rehr, J. J.; Zabinsky, S. I.; Albers, R. C. *Phys. Chem. B* **1991**, *44*, 4146. (23) (a) Rehr, J. J.; Mustre de Leon, J.; Zabinsky, S. I.; Albers, R. C. *J. Am. Chem. Soc.* **1991**, *113*, 5135. (b) Neese, F. ORCA, an Ab Initio, Density Functional, and Semiempirical Electronic Structure Program Package, version 2.8; Universit at Bonn: Bonn, Germany, 2011. (24) Becke, A. D. *Phys. Rev. A* **1988**, *38*, 3098. (25) Sch afer, A.; Horn, H.; Ahlrichs, R. *J. Chem. Phys.* **1992**, *97*, 2571. (26) Sch afer, A.; Huber, C.; Ahlrichs, R. *J. Chem. Phys.* **1994**, *100*, 5829. (27) (a) Becke, A. D. *J. Chem. Phys.* **1993**, *98*, 5648. (b) Lee, C.; Yang, W.; Parr, R. G. *Phys. Chem. B* **1988**, *37*, 785. (28) (a) Pulay, P. *Chem. Phys. Lett.* **1980**, *73*, 393. (b) Pulay, P. *J. Comput. Chem.* **1982**, *3*, 556. (29) Neese, F. *J. Phys. Chem. Solids* **2004**, *65*, 781. (30) Sch oneboom, J. C.; Neese, F.; Thiel, W. *J. Am. Chem. Soc.* **2005**, *127*, 5840. (31) Molekel, *Advanced Interactive 3D-Graphics for Molecular Sciences*; Swiss National Supercomputing Center; <http://www.cscs.ch/molkel>. (32) Klamt, A.; Jonas, V.; B urger, T.; Lohrenz, J. C. W. *J. Phys. Chem. A* **1998**, *102*, 5074. (33) The electronic structure and calculated X-ray absorption spectra of the cations [Cr(bpy)₃]^{3+,2+,1+} and [Cr(tacn)₃]^{3+,2+} are not significantly affected by the application of COSMO, whereas the electronic structure details of the anions [Cr(bpy)₃]^{1-,2-,3-} are. See the Supporting Information for details. (34) (a) Noodleman, L. *J. Chem. Phys.* **1981**, *74*, 5737. (b) Noodleman, L.; Case, D. A.; Aizman, A. *J. Am. Chem. Soc.* **1988**, *110*, 1001. (c) Noodleman, L.; Davidson, E. R. *Chem. Phys.* **1986**, *109*, 131. (d) Noodleman, L.; Norman, J. G.; Osborne, J. H.; Aizman, A.; Case, D. A. *J. Am. Chem. Soc.* **1985**, *107*, 3418. (e) Noodleman, L.; Peng, C. Y.; Case, D. A.; Mouesca, J. M. *Coord. Chem. Rev.* **1995**, *144*, 199. (f) Adams, D. M.; Noodleman, L.; Hendrickson, D. N. *Inorg. Chem.* **1997**, *36*, 3966. (35) DeBeer George, S.; Petrenko, T.; Neese, F. *Inorg. Chim. Acta* **2008**, *361*, 965. (36) DeBeer George, S.; Petrenko, T.; Neese, F. *J. Phys. Chem. A* **2008**, *112*, 12936. (37) Neese, F. *Inorg. Chim. Acta* **2002**, *337*, 181. (38) (a) Berry, J. F.; DeBeer George, S.; Neese, F. *Phys. Chem. Chem. Phys.* **2008**, *10*, 4361. (b) Yano, J.; Robblee, J.; Pushkar, Y.; Marcus, M. A.; Bendix, J.; Workman, J. M.; Collins, T. J.; Solomon, E. I.; DeBeer George, S.; Yachandra, V. K. *J. Am. Chem. Soc.* **2007**, *129*, 12989. (39) Wulf, E.; Herzog, S. *Z. Anorg. Allg. Chem.* **1972**, *387*, 81. (40) Hume, D. N.; Stone, H. W. *J. Am. Chem. Soc.* **1941**, *63*, 1200. (41) Elliott, N. J. *J. Chem. Phys.* **1967**, *46*, 1006.

- (42) König, E.; Kremer, S. *Chem. Phys. Lett.* **1970**, *5*, 87.
- (43) Chaudhuri, P.; Wieghardt, K. *Prog. Inorg. Chem.* **2007**, *35*, 329.
- (44) Ljungström, E. *Acta Chem. Scand.* **1977**, *A31*, 104.
- (45) Jagner, S.; Ljungström, E.; Vannerberg, N.-S. *Acta Chem. Scand.* **1974**, *A28*, 623.
- (46) (a) Saji, T.; Aoyagui, S. *J. Electroanal. Chem.* **1975**, *63*, 405. (b) Saji, T.; Aoyagui, S. *J. Electroanal. Chem.* **1975**, *60*, 1. (c) Sato, Y.; Tanaka, N. *Bull. Chem. Soc. Jpn.* **1969**, *42*, 1021.
- (47) (a) Hughes, M. C.; Rao, J. M.; Macero, D. J. *Inorg. Chim. Acta* **1979**, *35*, L321. (b) Hughes, M. C.; Macero, D. J. *Inorg. Chem.* **1976**, *15*, 2040.
- (48) McDaniel, A. M.; Tseng, H.-W.; Damrauer, N. H.; Shores, M. P. *Inorg. Chem.* **2010**, *49*, 7981.
- (49) Vlček, A. A. *Coord. Chem. Rev.* **1982**, *43*, 39.
- (50) (a) Tom Dieck, H.; Franz, K.-D.; Hohmann, F. *Chem. Ber.* **1975**, *108*, 163. (b) Josephsen, J.; Schäffer, C. E. *Acta Chem. Scand.* **1977**, *31A*, 813. (c) Hancock, R. D.; McDougall, G. J. *J. Chem. Soc., Dalton Trans.* **1977**, 67.
- (51) Kapre, R. R.; Bothe, E.; Weyhermüller, T.; DeBeer George, S.; Muresan, N.; Wieghardt, K. *Inorg. Chem.* **2007**, *46*, 7827.
- (52) Banerjee, P.; Sproules, S.; Weyhermüller, T.; DeBeer George, S.; Wieghardt, K. *Inorg. Chem.* **2009**, *48*, 5829.
- (53) Lord, R. L.; Schultz, F. A.; Baik, M.-H. *J. Am. Chem. Soc.* **2009**, *131*, 6189.
- (54) König, E. *Z. Naturforsch., A: Phys. Sci.* **1964**, *19*, 1139.
- (55) (a) Soda, T.; Kitagawa, Y.; Onishi, T.; Takano, Y.; Shigeta, Y.; Nagao, H.; Yoshioka, Y.; Yamaguchi, K. *Chem. Phys. Lett.* **2000**, 319, 223. (b) Yamaguchi, K.; Takahara, Y.; Fueno, T. In *Applied Quantum Chemistry*; Smith, V. H., Ed.; Reidel: Dordrecht, the Netherlands, 1986; p 155.
- (56) Rosa, P.; Mézailles, N.; Ricard, L.; Mathey, F.; Le Floch, P. *Angew. Chem., Int. Ed.* **2000**, *39*, 1823.
- (57) Nikiforov, G. B.; Roesky, H. W.; Noltemeyer, M.; Schmidt, H.-G. *Polyhedron* **2004**, *23*, 561.
- (58) Ray, K.; DeBeer George, S.; Solomon, E. I.; Wieghardt, K.; Neese, F. *Chem.—Eur. J.* **2007**, *13*, 2783.
- (59) Kapre, R.; Ray, K.; Sylvestre, I.; Weyhermüller, T.; DeBeer George, S.; Neese, F.; Wieghardt, K. *Inorg. Chem.* **2006**, *45*, 3499.
- (60) It is well-known that TD-DFT has severe problems modeling excited states with charge transfer character: depending on the system and the amount of Hartree–Fock exchange in the functional, such transitions can move by several electron volts while the 1s to 3d transitions are essentially unaffected. This is well-known from valence excited states in the UV and visible regions of the spectrum: (a) Neese, F. *J. Biol. Inorg. Chem.* **2006**, *11*, 702. (b) Tozer, D. J. *J. Chem. Phys.* **2003**, *119*, 12697. It also holds for XAS calculations: (c) Roemelt, M.; Beckwith, M. A.; Duboc, C.; Collomb, M.-N.; Neese, F.; DeBeer, S. Manuscript in preparation. Therefore, in order to best correlate our computational and experimental results, we focus on the well-resolved 1s to 3d feature.
- (61) Le Floch, P.; Carmichael, D.; Ricard, L.; Mathey, F.; Jutand, A.; Amatore, C. *Organometallics* **1992**, *11*, 2475.
- (62) (a) Kaizu, Y.; Kobayashi, H. *Bull. Chem. Soc. Jpn.* **1972**, *45*, 470. (b) Kaizu, Y.; Kobayashi, H. *Bull. Chem. Soc. Jpn.* **1970**, *43*, 2492.
- (63) Vlček, J. A.; Baumann, F.; Kaim, W.; Grevels, F.-W.; Hartl, F. *J. Chem. Soc., Dalton Trans.* **1998**, 215.
- (64) Zalis, S.; Daniel, C.; Vlček, A. *J. Chem. Soc., Dalton Trans.* **1999**, 3081.
- (65) (a) Scarborough, C. C.; Wieghardt, K. Unpublished results. (b) For DFT calculations for $[(\text{CO})_4\text{Cr}^{\text{I}}(\text{phen})]^+$ ($S = 1/2$), see: Farrell, I. R.; Hartl, F.; Zális, S.; Wanner, M.; Kaim, W.; Vlček, A. *Inorg. Chim. Acta* **2001**, *318*, 143.
- (66) (a) Sofen, S. R.; Ware, D. C.; Cooper, S. R.; Raymond, K. N. *Inorg. Chem.* **1979**, *18*, 234. (b) Raymond, K. N.; Isied, S. S.; Brown, L. D.; Fronczek, F. R.; Nibert, J. H. *J. Am. Chem. Soc.* **1976**, *98*, 1767. (c) Isied, S. S.; Kuo, G.; Raymond, K. N. *J. Am. Chem. Soc.* **1976**, *98*, 1763. (d) Pierpont, C. G.; Downs, H. H. *J. Am. Chem. Soc.* **1976**, *98*, 4834. (e) Buchanan, R. M.; Kessel, S. L.; Downs, H. H.; Pierpont, C. G.; Hendrickson, D. N. *J. Am. Chem. Soc.* **1978**, *100*, 7894.